Avalanches, hydrodynamics, and discharge events in models of sandpiles

Terence Hwa
Department of Physics, Harvard University, Cambridge, Massachusetts 02138

Mehran Kardar
Department of Physics, Massachusetts Institute of Technology, Cambridge, Massachusetts 02139
(Received 23 August 1991)

Motivated by recent studies of Bak, Tang, and Wiesenfeld [Phys. Rev. Lett. **59**, 381 (1987); Phys. Rev. A **38**, 364 (1988)], we study self-organized criticality in models of "running" sandpiles. Our analysis reveals rich temporal structures in the flow of sand: at very short time scales, the flow is dominated by single avalanches. These avalanches overlap at intermediate time scales; their interactions lead to $1/f$ noise in the flow. We show that scaling in this region is a consequence of conservation laws and is exhibited in many examples of driven-diffusion equations for transport. At very long time scales, the sandpiles exhibit system-wide discharge events. These events also obey scaling and are found to be anticorrelated. We derive the $f^{1/2}$ mean-field power spectrum for these events and show that a threshold instability of the model, coupled with some stochasticity, is the underlying origin of the long-time anticorrelation.

PACS number(s): 05.40.+j, 05.60.+w, 46.10.+z, 64.60.Ht

I. INTRODUCTION

We live in a world full of complex spatial patterns and structures such as coastlines and river networks [1]. There are similarly diverse temporal processes generically exhibiting "$1/f$" noise, as in resistance fluctuations [2], sand flow in hourglasses [3], and even in traffic and stock market movements [4]. These phenomena lack natural length and time scales and instead possess scale-invariant or self-similar features. The concept of fractals [1] has been successful in *characterizing* the geometrical aspects of scale-invariant systems, while methods developed from the studies of critical phenomena [5] may provide the necessary analytical tools. In static critical phenomena, scale invariance and self-similarity are only exhibited at a few isolated, or critical, points in the parameter space under study [5]. By contrast, many systems in nature can exhibit self-similarity without any tuning of parameters. For this reason, this generic behavior has been recently dubbed "self-organized criticality" (SOC) [6].

Usually the existence of an invariance (such as the above-mentioned self-similarity) is a consequence of a more general underlying cause. For example, in classical mechanics, the invariance of total momentum in a closed system results from translational symmetry in space. To gain some hint of such an underlying cause for SOC, let us examine some well-known systems encountered in statistical physics that show generic scale invariance [5,7]. A trivial example is provided by the dynamics of a diffusing field which can exhibit power-law correlation in both space and time (and is in this sense critical). Other less trivial examples include three-dimensional Heisenberg ferromagnets below their Curie temperature [7], and the morphology of growing interfaces [8]. We conclude from these examples some candidates for possible principles governing the scale invariances in SOC: The conservation of particle number is the origin of self-similarity of the diffusing field. In the case of the Heisenberg magnet, and the growing interface, the scale invariance is due to an infinitesimal symmetry (Goldstone modes [9] of rotation for the ferromagnet, and the capillary modes of translation for the interface).

Although magnets and growth problems have been widely used to demonstrate fractal structures, they are not natural systems for the investigation of temporal complexities such as $1/f$ noise [10]. Since these low-frequency fluctuations often make their appearance in transport processes, we may hope to gain some insights by studying such phenomena. This motivated the recent introduction of an interesting model of dissipative transport, the sandpile automaton, by Bak, Tang, and Wiesenfeld (BTW) [6]. The study reported here was inspired by the BTW model. In Sec. II we start with a brief description of the model and present detailed simulation results for "running" sandpiles in $1+1$ dimension. Analysis of the automaton and its outputs reveals various scaling regimes: (1) A short-time regime in which temporal fluctuations are dominated by isolated avalanches; (2) an intermediate hydrodynamic regime in which avalanches interact to provide rich temporal structures, resulting in $1/f$-type noise; and (3) an anticorrelated event regime due to system-wide discharges. The existence of the discharge events [11] is a unique feature of systems with threshold instabilities. We provide a simple description for the underlying mechanism of discharge-event generation. Similar behaviors are found in preliminary simulations of $(2+1)$-dimensional models. The generic behavior of the "running" sandpiles found in simulations actually bears an interesting resemblance to findings in recent experiments on real sand [12], and suggests some experimental implications.

In Sec. III we apply the formalism of dynamical renormalization group (DRG) [13] to the sandpile model by considering the fluctuation of its surface in the intermedi-

 ©1992 The American Physical Society

ate hydrodynamic region. We show in detail the construction of the equation of motion by recognizing the presence or absence of various symmetries, combined with conservation laws of the local dynamics. Scale invariance in this model is a consequence of the conservation law. We describe the extension of the traditional DRG methods to anisotropic systems such as the "running" sandpile, and show how scaling exponents for its surface can be calculated. We then established the connections to the exponents α of the $1/f^{\alpha}$-noise spectra for various transport quantities, and make a critical comparison with the numerical results. A discussion of various universality classes of SOC is given at the end.

II. THE SANDPILE MODEL

A. The automaton

Recent interest in the phenomena of SOC springs from a series of thought-provoking numerical studies on a sandpile cellular automaton invented by BTW [6]. The model raises some important issues regarding dissipative transport in open environments, and is certainly worthy of investigation. In this section, we describe the results of simulations of a version of the BTW sandpile with open boundaries. The numerical study is mostly limited to the $(1+1)$-dimensional case (a strip of sand), though the generic behavior found also seems to hold in higher dimensions.

We consider a sandpile defined on a one-dimensional lattice of length L. Associated with each lattice site n is an integer variable $H(n,t)$ representing the height of the local sand column (see Fig. 1). Following the generalization of the one-dimensional BTW model by Kadanoff *et al.* [14], we adopt the evolution rules

$$\begin{aligned} H(n,t+1)&=H(n,t)-N_f\ , \\ H(n\pm1,t+1)&=H(n\pm1,t)+N_f \end{aligned} \tag{1}$$

if and only if $H(n,t)-H(n\pm1,t)>\Delta$. As reported in Ref. [14], the scaling behavior of the system is independent of the numerical values of N_f and Δ as long as $N_f\geq 2$ and $\Delta\geq 2N_f$ in order to exclude certain pathological cases. In our study, we use $N_f=2$, and $\Delta=8$. The boundary at $n=0$ is kept closed, while the boundary at $n=L$ is open, i.e., $H(0,t)=H(1,t)$, and $H(L+1,t)=0$.

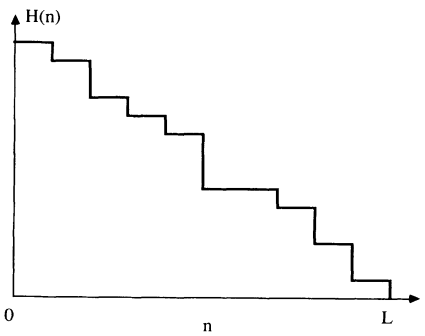

FIG. 1. A possible configuration of the $(1+1)$-dimensional sandpile automaton.

The system can be started from uniform or random initial conditions. The transport process is initiated by randomly depositing sand grains into the system at a rate J_{in}. After some time, the system reaches a steady state in which the input is on average balanced by the drainage at the open end. The activity of the system is then monitored by recording the output current $J(t)$ (the number of sand grains leaving the system) and the instantaneous energy dissipation rate $E(t)$ (the total number of transport activities at each time step).

We first briefly summarize previous results of similar simulations. BTW performed numerical studies of the sandpile model in the limit of zero deposition rate, i.e., $J_{\text{in}}\to 0+$. In this limit, the response to a single addition of a sand grain is characterized by identifying the size $[s=\int E(t)dt]$ and duration (T) of the "avalanche" resulting from the addition. In the steady state, BTW identified the signatures of criticality: power-law scaling in the distributions of the quantities monitored, i.e.,

$$D(T)=T^{-y}F(T/L^{\sigma})\ , \tag{2}$$

$$D(s)=s^{1-\tau}G(s/L^{D_f})\ , \tag{3}$$

where $D(X)$ is the distribution function for X. Finite-size scaling then yields the dynamical exponent σ, and the "fractal dimension" of avalanches, D_f. In fact, the distribution functions may well be more complicated, e.g., multifractal, as indicated in Ref. [14]. But these simple scaling laws work well for $s\ll L$. (The multifractal aspects will be discussed later.)

Tang and Bak (TB) [15] suggested that the scaling behaviors observed can be thought of as critical phenomena with the average output current $\langle J_{\text{out}}\rangle$ being an order parameter. The sandpile model adjusts itself (self-organizes) to a critical slope at which $\langle J_{\text{out}}\rangle\to 0+$. TB also pointed out that if $\langle J_{\text{in}}\rangle$ is finite, then the large avalanche clusters overlap (much like a percolating system beyond the percolation threshold), resulting in a length scale $\xi\sim J^{-\nu}$ and an associated time scale $\sim\xi^{\sigma}$, above which the power-law distributions are cut off. The existence of such scales would apparently destroy scale invariance and criticality.

Aware of the above arguments, most subsequent studies [14–19] focused on the special limit $J_{\text{in}}\to 0+$ by adding sand grains one at a time and allowing the system to completely relax between additions. Although many interesting scaling behaviors were found, there are a number of drawbacks associated with this particular way of probing the system. For instance, as the interval between sand additions varies, time is not well defined in these studies, and temporal fluctuations of transport quantities are constructed artificially by randomly superposing signals taken from the relevant distribution functions. The resulting outputs exhibit very smooth fluctuations and no sign of $1/f$ noise [20,21]. This is somewhat disappointing since a natural explanation for $1/f$ noise was one of the early motivations of SOC studies. Another shortcoming stems from the very insistence on the limit $J_{\text{in}}\to 0$. By the definition of the steady state ($\langle J_{\text{out}}\rangle=\langle J_{\text{in}}\rangle$), the order parameter $\langle J_{\text{out}}\rangle$ is indirectly *tuned* by $\langle J_{\text{in}}\rangle$. If

the existence of criticality depends so sensitively on a very small input rate (or driving force), it becomes inapplicable to many systems in nature (e.g., water flow in rivers [22] and electron flow in resistors [2] that exhibit $1/f$-type noise in the presence of obvious driving forces. One conclusion of this numerical study is that in fact critical scaling is *not* destroyed by a finite driving force; rather, we show that interesting temporal fluctuations such as $1/f$ noise only appear when avalanches overlap in the presence of increased external driving force J_{in}.

Let us first quantify how small J_{in} must be for avalanche clusters to overlap each other: If we mark all the sites where the local slope exceeds the transport threshold, then an avalanche in the one-dimensional model shows up as a parallelogram in the space-time plane (Fig. 2). The width at each time t is the number of active sites $E(t)$. (This is also the instantaneous rate of energy dissipation since the particles lose potential energy every time they are transported.) The length of the parallelogram is the avalanche duration T, and the total shaded area is the total size of the avalanche cluster s. Two clusters can be distinguished as long as their *active* zones never overlap. If the probability of initiating an avalanche (the local deposition rate) is p per site, then clusters do not overlap if $\bar{s}p < 1$, where $\bar{s}$ is the average size of the clusters. For a system of size L, $\bar{s} = L^{D_f(3-\tau)}$ from the distribution function Eq. (3). It is found in Ref. [14] that $\tau \approx 2$ and $D_f \approx 1$ for the one-dimensional (1D) sandpile, giving $\bar{s} \sim L$ and the overlap limit

$$p < L^{-1} . \tag{4}$$

In the following, we describe the simulation results for "running" sandpiles in which sand grains are deposited with probability $p = J_{\text{in}}/L$ per site per time step, and the total input current J_{in} is fixed for different system sizes. (The reason for the choice of dependence on size will be given shortly.) By changing the magnitude of the driving force J_{in}, we can probe both below and above the avalanche-overlap limit, Eq. (4). It is shown that interesting temporal fluctuations such as $1/f$ noise appear only for driving forces *exceeding* the limit set in Eq. (4).

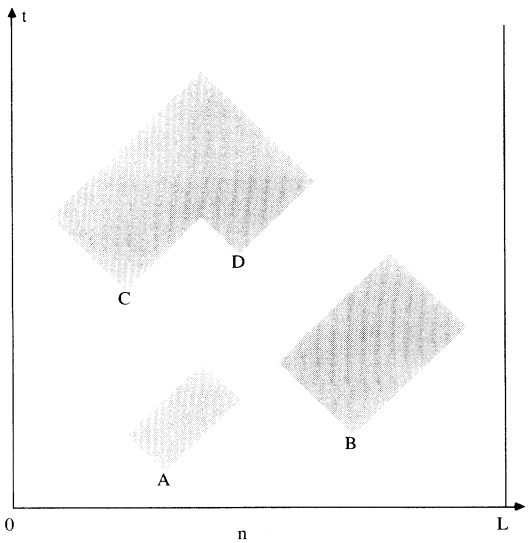

FIG. 2. One-dimensional avalanche processes represented in a space-time diagram. The two avalanches initiated at points A and B are considered independent because they do not overlap in space time. The two initiated at points C and D, however, do overlap.

B. The "running" sandpile

In this simulation, discrete "sand grains" are randomly added to the system. Time is defined by an external clock. At each time step, there is a small probability p of depositing a particle to each site, i.e., $H(n,t+1) = H(n,t)+1$ with probability p. The configuration $H(n)$ is *simultaneously* updated according to Eq. (1). (A random asynchronous updating procedure has also been tested and does not change the generic behavior.) There is an average deposition rate $J_{\text{in}} = pL$ for a system of size L. We let the system evolve for a long time until the steady state is reached, i.e., $\langle J_{\text{in}} \rangle = \langle J_{\text{out}} \rangle$. In steady state, we record the time series for the output current $J(t)$ and the instantaneous energy dissipation $E(t)$ as previously defined. We then take the power spectra $S_J(\omega)$ and $S_E(\omega)$ for the output series, where

$$S_X(\omega) = \int dt \int d\tau\, e^{-i\omega\tau} X(t) X(t+\tau) .$$

If the avalanches do not overlap, then according to BTW, the resulting time series should be equivalent to the random superposition of single avalanches according to the relevant distribution functions in Eqs. (2) and (3). In particular, the power spectrum of the output current is predicted [20,21] to have the form $S_J(\omega) \sim \omega^{-\beta} F(\omega L^{\sigma})$ where $\beta = 3-y$ for $y > 1$, $\beta = 2$ for $y < 1$, and $F(x)$ is a cutoff function due to the finite size. Thus $1/f$-type noise *may* arise as a consequence of random superposition of individual avalanches, provided that the avalanche lifetime distribution does not have too long a tail. However, one does not expect temporal correlations beyond a time scale set by the duration of the longest avalanche, i.e., $S(\omega) = \text{const}$ for $\omega < L^{\sigma}$.

This is indeed the case when we directly analyze the output time series for systems subject to very small driving forces: To ensure that the avalanches do not overlap, we deposit at an average of one grain every 1000 time steps to a system of 100 sites (for which the largest avalanche lasts ≈ 100 steps). Figure 3 shows the resulting power spectra from which we obtain the exponents $\beta_E \approx 4$ and $\beta_J \approx 2$. Clearly, the power spectra do not exhibit $1/f$-type broadband noise. This result agrees with other recent studies [20,21] in which the power spectra are obtained directly from the distribution functions assuming random superposition of signals.

As many transport systems in nature do have non-negligible driving forces, we next investigate the robustness of the scaling behaviors found above by exciting the avalanches more frequently. Following TB [15], one may expect the cutoffs to the scaling regions in Fig. 3 to move to higher frequencies (or shorter times) due to the overlap of large avalanches, so that in the large-input-rate limit, the scaling region is drastically reduced and scale invariance is lost in the macroscopic limit. However, when we repeat the simulation at higher input rates, we obtain the

interesting series of power spectra shown in Fig. 4. While the cutoff times are indeed reduced due to more frequent avalanche overlaps, new scaling regions with $S(\omega)\sim\omega^{-1}$ seem to emerge at a time scale beyond the cutoff.

We next describe a systematic study of the behavior of the sandpile in the overlapping avalanche limit by examining the size dependence of the power spectra. At this point, it is important to mention that the sandpile model in Eq. (1) has a limited maximum output capacity of N_f grains per time step independent of the system size. Driving the system beyond this limit will saturate it and give meaningless results. Therefore for the following study, we chose to fix the input rate at $J_{\rm in}<N_f$ independent of the system size. This implies that the local deposition rate $p=J_{\rm in}/L$ is size dependent. It is used here for the purpose of *illustrating* the behavior of flow beyond the avalanche overlap limit. Using $J_{\rm in}=0.1$, the resulting power spectra for systems of sizes ranging from 25 to 800 are shown in Fig. 5. The power spectra exhibit a variety of different behaviors depending on the time scale of observation. They are qualitatively divided into three nontrivial regions as sketched in Fig. 6 and the relevant exponents are listed in Table I. We now describe each region in detail.

1. *The single-avalanche region*

In this high-frequency region (I), the observation time is of the order of the avalanche duration. The power spectra are described by the scaling forms, $S_E(\omega,L)=\omega^{-\beta_E}F(\omega L^{\sigma'})$ and $S_J(\omega,L)=\omega^{-\beta_J}L^{-0.5}F(\omega L^{\sigma'})$ where $\beta_E\approx 4$, $\beta_J\approx 2$, and $\sigma'\approx 0.5$ [23]. Note that S_J decreases with the system size L in this region. [The vertical axis of Fig. 5(b) is scaled by $L^{0.5}$.] To gain some understanding of this scaling region, we directly examine the time series. Figure 7 shows some typical time series of the instantaneous energy dissipation $E(t)$ at the time scale of region (I) for systems of size 25 and 800. We recognize the activities shown to be the superposition of individual avalanche signals. The smoothness of the time series is a direct result of addition of many random signals; this is reflected in the large value

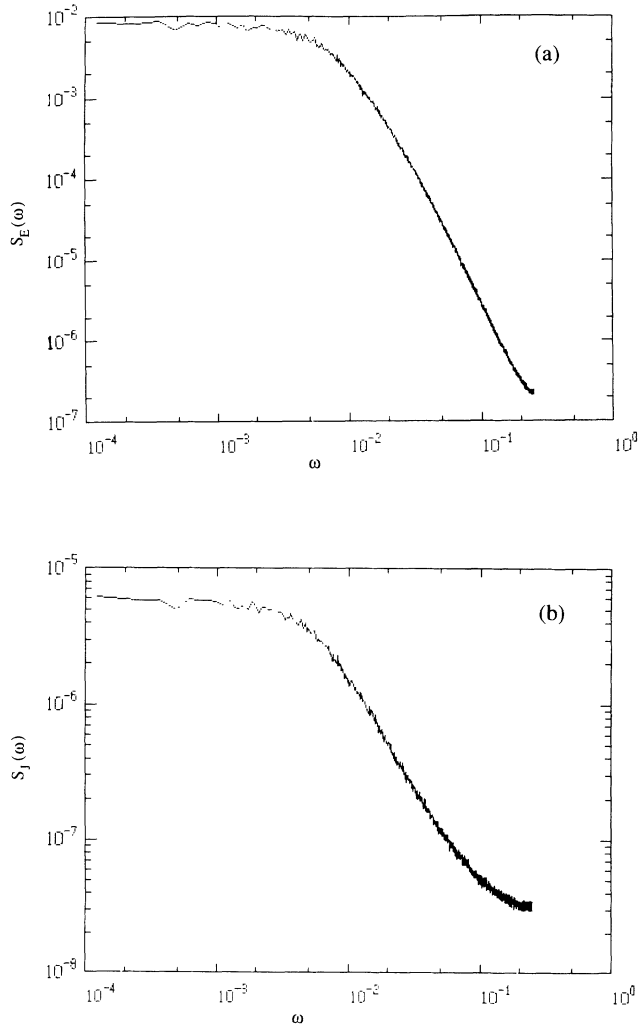

FIG. 3. Power spectra for energy dissipation and output current of a 100-site system, with $p=10^{-5}$.

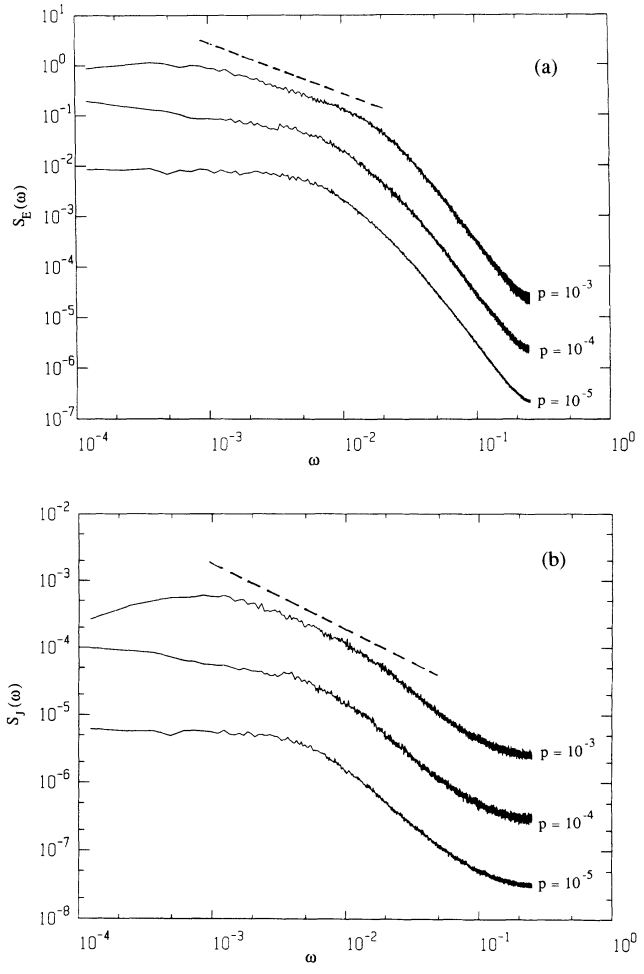

FIG. 4. Power spectra of (a) the energy dissipation and (b) the output current for a one-dimensional sandpile ($L=100$) with deposition rates $p=10^{-3}$, 10^{-4}, and 10^{-5} per site. Notice that a new scaling region emerges as we increase the input rate. [Dashed lines indicate $S(\omega)\sim\omega^{-1}$.]

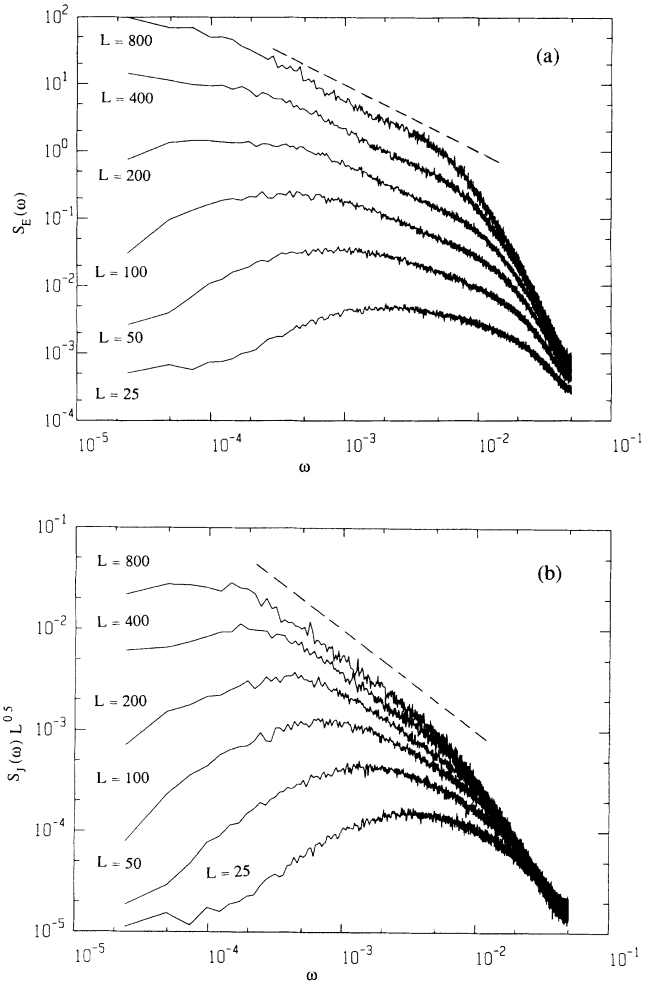

FIG. 5. Power spectra of the one-dimensional sandpile in Eq. (1) for (a) the energy dissipation $E(t)$, and (b) the output current $J(t)$. Note that the vertical axis of (b) is scaled by $L^{0.5}$. [Dashed lines indicate $S(\omega)\sim\omega^{-1}$.]

of the exponent β_E. We also see from Fig. 4 that the high-frequency scaling behavior for systems with large deposition rate is the same as that with small deposition rate for which avalanche overlap is not possible. We therefore conclude that this region corresponds to the random superposition of *independent* avalanches. Although the form of power spectra in this region is rather simple, the scaling behaviors of the distribution functions themselves are highly nontrivial [24–26] and challenge theoretical understanding.

The upper cutoff time T_A for region (I) is not very long even if the avalanches never overlap; it has an upper bound of the maximum lifetime of one avalanche, i.e.,

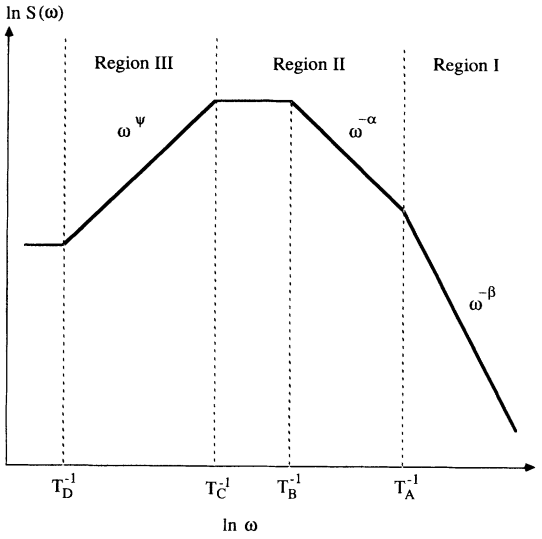

FIG. 6. Qualitative behavior of power spectra shown in Fig. 6.

$T_A \leq L^{\sigma}$, where the dynamic exponent σ is typically less than unity for a decelerating process. To put it in the perspective of a real avalanche process such as an earthquake, T_A could be the duration of one quark which may last seconds to minutes. While the way energy is released during one quake is certainly worthy of study, we need to look at longer time scales for purposes of investigating long-time fluctuations such as $1/f$ noise observed in river flow, resistors, and in aftershocks after major quakes.

2. *The interacting avalanche region*

We now come to a major result of this numerical study. Far from being uncorrelated as previously thought [15], the transport quantities exhibit $1/f$ noise at time scales beyond the maximum duration of individual avalanches. In this region (II), the power spectra can be fitted to power laws of the form $S_X(\omega)=\omega^{-\alpha_X}$. The exponents are determined to be $\alpha_E \approx 1.0$, and $\alpha_J \approx 1.0$ (using the results of $L=400,800$ systems in Fig. 5). The cutoff time T_B for region (II) (see Fig. 6) is expected to be related to the system size L through another dynamical exponent, z [27]. This exponent cannot be determined adequately from the existing data, but may be accessible via analytical treatments such as the one given in Sec. III.

A more intuitive feel for this region is obtained by directly examining the time series coarse grained to the relevant scale, as in Fig. 8, for a system with 800 sites. It is clear that this series is characteristically different from that shown in Fig. 7, as the fluctuations are more erratic (less smooth), but not random—signature of $1/f$ noise.

TABLE I. A summary of scaling exponents found in various regions for the (1+1)-dimensional sandpile model. The exponents are defined in Fig. 6.

	Region III	Region II	Region I
Exponents for current	$\psi_J=1.0$	$\alpha_J=1.0$	$\beta_J=2.0$
Exponents for energy	$\psi_E=1.0$	$\alpha_E=1.0$	$\beta_E=4.0$

Since the time scales of these fluctuations are long compared to the maximum lifetime of single avalanches, we conclude that the correlations in this part of the spectrum must arise out of interactions among the avalanches. In this way, this region is reminiscent of aftershocks in earthquakes and shock waves in hydrodynamics (and is sometimes called the hydrodynamic region). It is therefore natural to resort to continuum field theory for a possible description of this behavior. As this is the relevant region for studies of $1/f$ noise, we shall provide a detailed analysis in Sec. III. It will be shown that the existence of power-law scaling in the hydrodynamic region is a consequence of the conservative dynamics present in the model. Again, we put these time scales into perspective by making analogies with earthquakes: aftershocks and correlations of quakes along a faultline can exist at time scales ranging from minutes to years.

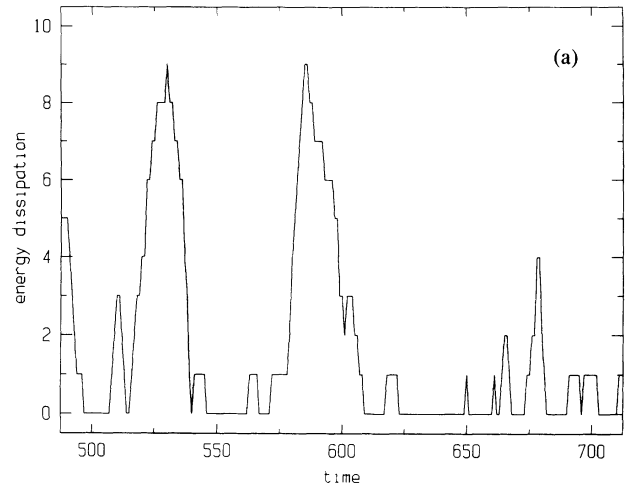

FIG. 7. Time series for instantaneous energy dissipation $E(t)$ of the one-dimensional sandpile with (a) $L=25$, and (b) $L=800$. Individual avalanche events can be identified at this time resolution.

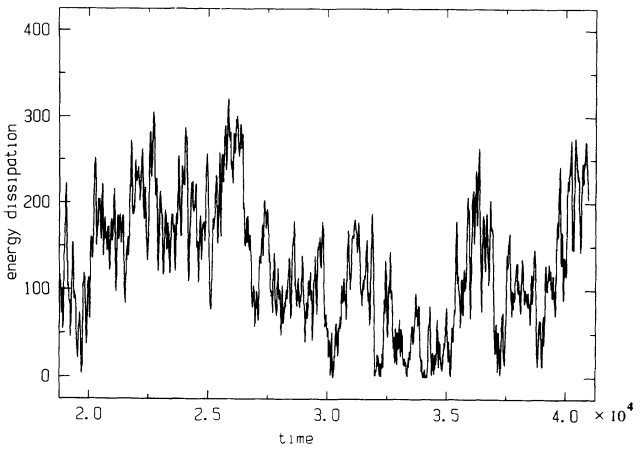

FIG. 8. Time series for instantaneous energy dissipation $E(t)$ of the one-dimensional sandpile with $L=800$. At this time resolution, correlation among avalanches can be seen.

3. *The discharge-event region*

When we look at even longer time scales, we encounter avalanches whose active zones are of the order of the system size (see Fig. 9). These great events sweep through the entire system and are thought to be system-wide discharge processes. The origin of discharge events has been studied by Carlson and Langer in a model of earthquakes [11], and has been alluded to in Ref. [14]. It can be traced back to a conservation law which we illustrate in the context of this model. For a sandpile of size L, the average input rate is fixed (i.e., $\langle J_{\text{in}} \rangle \sim 1$) while the scaling of output current can be determined from Fig. 5 to be $J_{\text{out}} \sim L^{-0.25}$ at short time scales. The sandpile is therefore accumulating particles at a constant rate. This process becomes impossible to ignore when the number of particles accumulated reaches the order L^2 (at which point the macroscopic slope of the sandpile is changed).

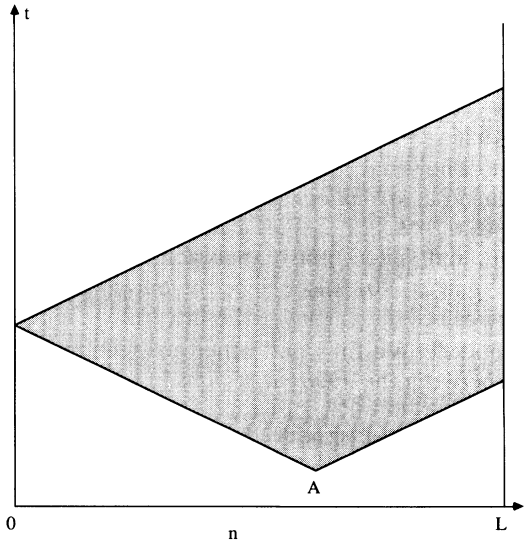

FIG. 9. A space-time diagram for a discharge event initiated at point A.

Thus beyond a time scale T_C (see Fig. 6) of the order L^2, a system-wide discharge process is bound to take place [28]. However, we have not had enough statistics to determine the precise L dependence of discharge-event sizes. Here we can only place a bound in the onset time, $L \leq T_c \leq L^2$. (Note that from Fig. 9 one obtains a discharge duration of the order L for a great event; this should not be confused with the correlation time between great events.) The scaling behavior of the great events will be discussed in detail in Sec. II C. It is important to recognize that the accumulation of particles at short-time scales is possible in the sandpile model due to the threshold nature of the dynamics which provides a multitude of metastable states. These behaviors should be contrasted with more conventional viscous fluid flows which do not exhibit the discharge activities observed here.

The effect of large-scale discharges can also be detected if one only looks at the avalanche distribution function $D(s)$. Because the large s part of the distribution is now subject to a different process and weighted more, we do not expect $D(s)$ to obey the simple, homogeneous scaling form in Eq. (3). As it turns out, the large avalanche end of the distribution is also scale invariant. Furthermore, the small and large size ends of the distribution $D(s)$ must be related. It is found numerically [14] that the entire distribution function is well described by a multifractal scaling form, though the implication of this remains to be understood.

Although the description of various scaling regions given above is based on results of the 1D sandpile, its generality goes beyond 1D systems. We have also performed the generalization of the rule in Eq. (1) on two-dimensional lattices. Due to the presence of anisotropy, a systematic study in 2D is much more demanding and has not been pursued here. In Fig. 10, we show some typical power spectra for $E(t)$. It appears that the qualitative behavior is the same as those described for the 1D system (Figs. 5 and 6). Power-law scaling is clearly seen in regions I and III, though much larger systems are needed to determine the behavior in the intermediate hydrodynamic region.

The sandpile thus behaves like a complicated filter which takes a random white noise input $J_{\text{in}}(t)$ and converts it into a highly correlated output $J_{\text{out}}(t) = \int_{-\infty}^{t} dt' G(t-t') J_{\text{in}}(t')$, where G is a delayed response function. The usual constraints of a causality and conservation then put strong constraints on the power spectrum $S_J(\omega) = |\tilde{G}(\omega)|^2 \langle J_{\text{in}}^2 \rangle_c$. For example, $J_{\text{out}} = J_{\text{in}}$ implies $\tilde{G}(0) = 1$, and $S_J(\omega)$ must approach a constant value, $\langle J_{\text{in}}^2 \rangle_c = p$ as $\omega \to 0$. Also, since the output current is always finite, i.e., $J_{\text{out}}(t) \leq N_f$, the integral $\int_0^\infty d\omega S_J(\omega)$ is also bounded. We thus find other connections and constraints between the different regions in Fig. 6.

C. Scaling of the discharge events

Let us return to the power spectrum shown in Fig. 5. It can be seen from the low-frequency behavior of the small systems that temporal fluctuations in the discharge-event region are not uncorrelated. The power spectra can be described by $S_X(\omega) \sim \omega^{\psi_X}$ where

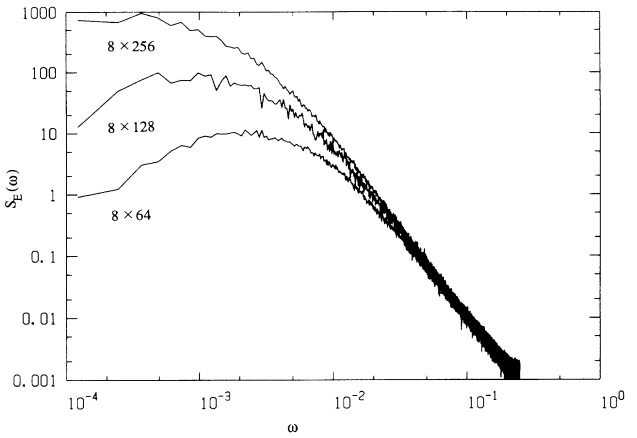

FIG. 10. Power spectrum for the energy dissipation $E(t)$ of several two-dimensional lattices. The choice of narrow strip geometry is due to the presence of strong anisotropy (see Sec. III).

$\psi_E \approx \psi_J \approx 1$; the positive exponent indicates the presence of anticorrelations which persists for a long time. For instance, anticorrelation is present for a 25-site system up to a time $T \sim 10^4$. Where might such long-term correlations (memory effects) come from?

Since these events are system-wide discharges, we examine the time evolution of the macroscopic profile of the sandpile. Figure 11 illustrates a snapshot of a typical profile which is rather smooth and linear. We can then follow evolution of such a profile by simply tracking the time dependence of its slope (or the height of the first column). In Figs. 12(a) and 12(b), we show the slope movement coarse grained to below and above the onset time of the discharge. Clearly, the slope is quasistationary at small time scales, but executes stochastic motion at large time scales. Therefore we see that the anticorrelated region is related to the motion of the overall landscape of the system. This motion is in turn a consequence of particle accumulation as already mentioned.

To uncover the underlying mechanism of scaling in the

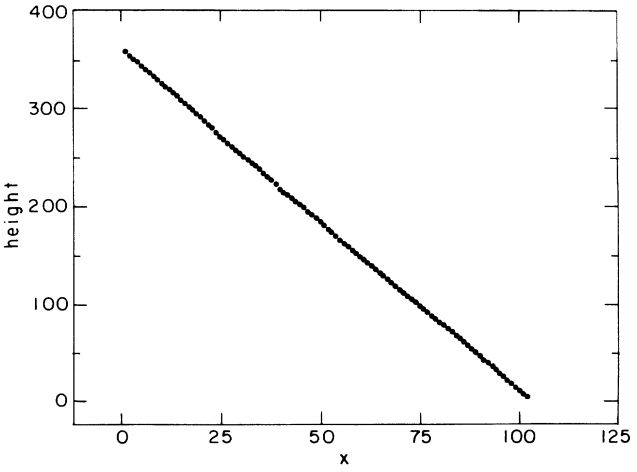

FIG. 11. A typical height profile for a sandpile ($L = 100$) in steady state.

anticorrelated discharge-event region, we analyze the global behavior of the system in the long-time limit by only keeping track of the total number of particles (N) accumulated. Coarse grained to the appropriate time scale of the discharge-event region, the system receives an average input of one unit per time step plus a small fluctuation $r(t)$ which is a Gaussian noise. We make a simplifying assumption that the system outputs a *fixed* amount of particles (N_f) once N reaches a certain threshold For the sake of illustration, let $N_f=10$ units. Then on average there is one output pulse every ten time steps. The inclusion of the small noise $r(t)$ in the input can shift the output series: Suppose N is at a value of $\epsilon=0^+$ above the threshold at some time, then there is immediately an output pulse, and we expect another output pulse to follow after ten time steps. However, if the magnitude of the accumulated noise within this time period is $-\delta$ where $\delta>\epsilon$, then N will be slightly *below* the threshold after ten time steps, and there will not be an output pulse until the 11th step. Similarly, if the random noise changes N from slightly below to slightly above the threshold in those ten time steps, the output pulse is advanced by one time step.

It is important to recognize that as long as the amplitude of the fluctuation $r(t)$ is small, it is extremely unlikely that the output sequence will have two consecutive delays or advances. This point may be better appreciated graphically: The modulation of the output sequence by a small noise is illustrated in Fig. 13. The output is delayed or advanced by one time step if the accumulated noise (a random walker for simple white noise) is on different sides of the origin between two output pulses. A simple, coarse-graining procedure transforms the actual output profile $J(t)$ to $\tilde{J}(t)$ as shown in Fig. 13(b). The function $\tilde{J}(t)$ more clearly represents the relation between the output sequence and zero crossings of the random walker: $\tilde{J}(t)=+1$ for upward crossings, and $\tilde{J}(t)=-1$ for downward crossings. It is apparent from Fig. 13 that the output sequence for this simple one-site model is anticorrelated: Every positive pulse is followed by a negative pulse. We can quantify this anticorrelation by calculating the correlation function $\langle\tilde{J}(0)\tilde{J}(t)\rangle$. Take $\tilde{J}(0)=+1$, the correlation function may be calculated by noting that the time series $\tilde{J}(t)$ can be written as $\tilde{J}(t)=dJ'(t)/dt$ (see Fig. 13) where

$$J'(t)=\begin{cases}+1 & \text{if } \int_0^t r(t')dt'>0\\ 0 & \text{if } \int_0^t r(t')dt'<0\ ,\end{cases}$$

and $r(0)=0$, $r'(0)>0$) by the choice of $\tilde{J}(0)$. So we have $\langle\tilde{J}(0)\tilde{J}(t)\rangle=(d/dt)\langle J'(t)\rangle$ where $\langle J'(t)\rangle$ is simply the probability of a random walker's return to the origin after a long time, which is well known ($\sim 1/\sqrt{t}$). Thus

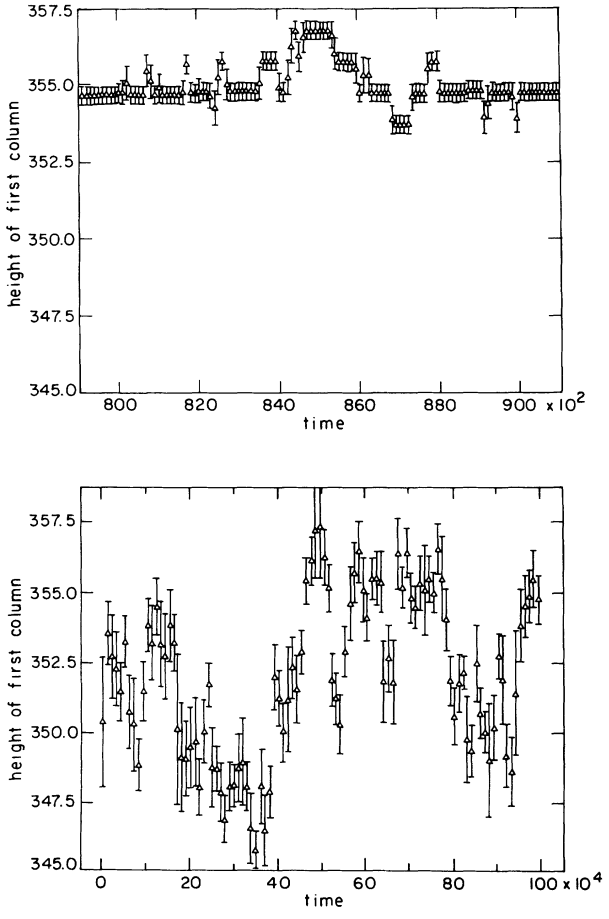

FIG. 12. Time dependence of the height of the first column at time scales (a) below and (b) above the onset time (T_C) of discharge events.

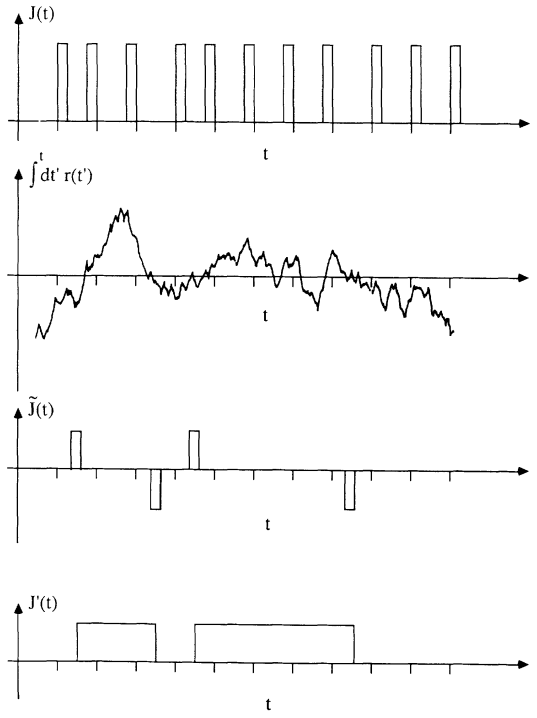

FIG. 13. The output sequence $J(t)$ of the one-site system due to a random noise shown below it. The coarse-grained output series is obtained from $\mathbf{J}(t)=\sum_{i=1}^{\tau}J(t+i)/\tau-J_{\text{in}}$, where $\tau=10$ is the average number of time steps between two output pulses and $J_{\text{in}}=1$. $\mathbf{J}(t)$ can also be thought of as the time derivative of the function $J'(t)$ shown at the bottom.

the correlation function is $\langle J(0)J(t)\rangle \sim t^{-3/2}$, yielding a power spectrum of $S(\omega)\sim\omega^{1/2}$. The behavior of such a one-site system has been simulated, and the power spectrum obtained (Fig. 14) is $\omega^{1/2}$ as calculated. (The anticorrelation is eventually cut off beyond a time scale when the random walker wanders to a value of the order of the input size). For the real system under study, the output pulse is of course not limited to a fixed size. A power-law distribution in output pulse sizes will then modify the exponent of the $\omega^{1/2}$ anticorrelation.

The above analysis suggests that the occurrence of great events should be common to a wide variety of driven systems that possess threshold instabilities. In particular, we note that some indications of the anticorrelated scaling behavior are seen in the power spectrum of the real sand flow [12]. As reported in Ref. [12], real sand shows relaxational oscillation between two angles ($\theta_{\min}$ and $\theta_{\max}$) when it is randomly added from above. This bears some superficial resemblance to the behavior of the one-site problem just considered; but upon more careful inspection the two systems are believed to be very different. According to Ref. [12], the slope of the real sand is *reset* to $\theta_{\min}$ once a threshold is exceeded, whereas in the one-site system, a *fixed* amount is output so that the system still retains some memory of the previous state after discharge. The above analysis shows that it is in fact this memory retention that is responsible for the anticorrelated scaling. Long-term anticorrelation is not possible if the slope is reset after each discharge event. Therefore, if an anticorrelated scaling region indeed exists for the real sand flow, it suggests that a small amount of memory retention may exist in the real sandpile after all, in which case the automata may actually give a fair description of very large sandpiles. Clearly, much better experimental knowledge of the low-frequency end of the power spectrum is needed if any concrete correspondence is to be made.

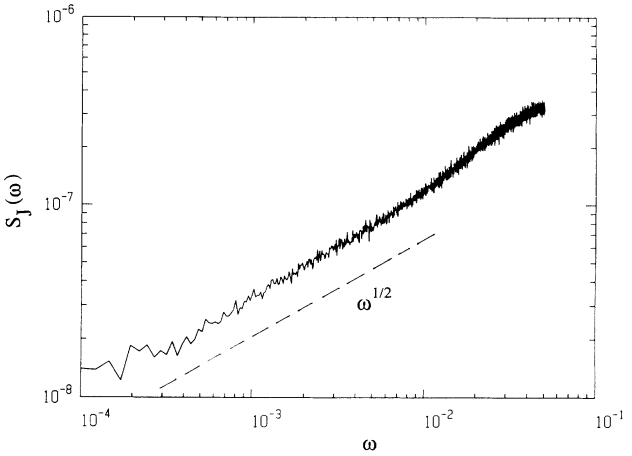

FIG. 14. The output power spectrum of a one-site system. The evolution rule used is as in Eq. (1) with $N_f=10$. The input used is $J_{\text{in}}=1+r(t)$ where $r(t)$ is randomly distributed in the interval -0.1 to 0.1.

III. FIELD THEORY OF DISSIPATIVE TRANSPORT

A. The driver-diffusion equation

We now consider the "running" sandpile model of Sec. II and investigate its behavior in the region of interacting avalanches by using the methods of hydrodynamics. To study this region we first coarse grain the system both in space and time to remove the small distance cutoffs (single avalanches) and obtain a coarse-grained landscape $\tilde{H}(\mathbf{x},t)$. The coarse-grained unit cell length l_0 and unit time t_0 must be large compared to the length scale at which deceleration of individual avalanches takes place. (According to the finite-size scaling summarized in Fig. 5, we need $l_0\sim t_0 > T_A \sim L^{1/2}$.) Also, as suggested from the numerical study in Sec. II, we assume the average landscape of the sandpile to be flat and stationary in the hydrodynamic region. (The assumption will be checked later for self-consistency.) We may now consider the avalanche dynamics from the point of view of fluctuations of the sandpile surface [29].

We define a dynamical field $h(\mathbf{x},t)$ which is the difference between the coarse-grained landscape $\tilde{H}(\mathbf{x},t)$ and the flat average profile $H_0(x)=\lambda_0(L-x)$, as shown in Fig. 15. The operation of the sandpile automaton consists of a driving action (addition of sand), and a subsequent relaxation according to Eqs. (1). We now note the important constraint that *the relaxation dynamics during an avalanche does not change the number of particles,* while the driving operation violates this conservation by adding particles randomly from the outside. Based solely on the above condition, we conclude that the equation of motion must take the form

$$\frac{\partial h}{\partial t}+\nabla\cdot\mathbf{j}(h)=\eta(\mathbf{x},t)\ . \tag{5}$$

The left-hand side of the equation represents the conservative (and deterministic) relaxation that follows the addition of particles, while the right-hand side represents the external sources and sinks in terms of a random input function η.

Next, we need a constitutive condition to describe the transport current $\mathbf{j}(h)$. For the complex nonequilibrium problem at hand there is no easy way to calculate $\mathbf{j}(h)$, but *it must satisfy the underlying symmetries of the problem.* Thus to construct the most general functional form possible for $\mathbf{j}(h)$ we closely examine the presence or absence of various symmetries. The anisotropic boundary conditions of the automaton pick out a direction of transport $\hat{\mathbf{T}}$. Let $\mathbf{x}_{\parallel}=(\hat{\mathbf{T}}\cdot\mathbf{x})\hat{\mathbf{T}}$ and $\mathbf{x}_{\perp}=\mathbf{x}-\mathbf{x}_{\parallel}$ denote directions

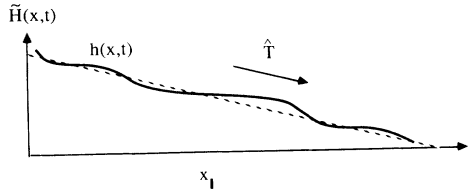

FIG. 15. The height function $h(\mathbf{x},t)$ is defined as a deviation from the flat steady-state sand profile. Gravity drives sand along the transport direction $\hat{\mathbf{T}}$.

parallel and perpendicular to $\hat{\mathbf{T}}$, respectively. Then the system has (a) *rotational invariance in* $\mathbf{x}_\perp$ *and translational invariance in* $\mathbf{x}_\perp$, $\mathbf{x}_\parallel$; but it (b) *lacks reflection symmetries in* $x_\parallel$ *and in* h because of the presence of a preferred direction $\hat{\mathbf{T}}$. However, with respect to the average flat surface "bumps" move downhill while "voids" move uphill as illustrated in Fig. 16. We therefore have (c) *the joint reflection symmetry* $h \to -h$ *and* $x_\parallel \to -x_\parallel$. Finally, we assume that (d) *the system lacks translational symmetry in* h as h measures the deviation from the average slope which is fixed once the input rate, the threshold, and the box size are specified. This last assumption is not always valid. In particular according to the evolution rules in Eq. (1), the current only depends on the difference between heights, and hence invariant under a uniform shift in h. A mechanism for spontaneously breaking this symmetry was recently suggested by Grinstein and Lee [30], and relies on the discreteness of the heights. For real sandpiles long-range interactions cut off by the box edges may provide such a mechanism. Our justification is also partly *a posteriori* based on the numerical profile in Fig. 11. Since the current is a vector, it must be constructed from ∇ and $\hat{\mathbf{T}}$, the only vectors in the problem by (a) and (b). Assuming (d) it can depend directly upon h, and (for *local* processes) takes on the general form

$$\begin{aligned}\mathbf{j}(h) = &-a_1\nabla h - a_2\nabla(h^2) - \cdots - a_n\nabla(h^n) \\ &- b_n\nabla(\nabla h)^{2n} - c_n\nabla(\nabla^2 h)^n + \cdots + \lambda_1 h\hat{\mathbf{T}} \\ &+ \lambda_2 h^2\hat{\mathbf{T}} + \cdots + \lambda_n(h^n)\hat{\mathbf{T}} + v_n(\nabla h)^{2n}\hat{\mathbf{T}} \\ &+ w_n(\nabla^2 h)^n\hat{\mathbf{T}} + \cdots .\end{aligned}$$

We are interested in the large-distance ($k \to 0$) properties of the system. In this limit, the term a_2 can be neglected compared to λ_2 because the former involves an extra spatial derivative. Similarly, the terms b_n and c_n are ignored when compared to v_n and w_n, respectively, and the v_n and w_n are themselves small compared to the λ_n terms. As to the remaining terms $\lambda_n h^n\hat{\mathbf{T}}$, we expect the fluctuations of h to be small if the surface is flat as initially assumed. (The self-consistency of this assumption can be checked when the scaling behavior of h is calculated.) Therefore higher-order terms in h are also ignored, and we have

$$\mathbf{j}(h) = -a_1\nabla h + \lambda_1 h\hat{\mathbf{T}} + \lambda_2 h^2\hat{\mathbf{T}} ,$$

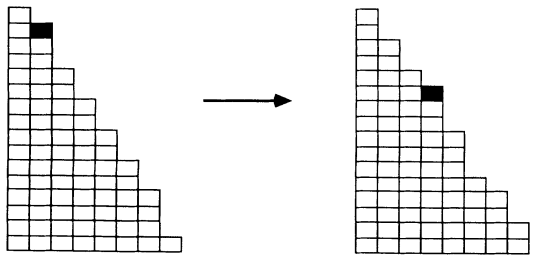

FIG. 16. The joint inversion symmetry $h \to -h$ and $x_\parallel \to -x_\parallel$: $+h$ (filled block) moves down the slope while $-h$ (void, shaded block) moves uphill.

to leading order. Of course the terms with a_1 and λ_2 are also small compared to the λ_1 term, except that the latter forbidden by the joint inversion symmetry (c). Of the two remaining terms, $\lambda_2 \equiv \lambda/2$ is the driving force proportional to the slope of the average flat surface; this term originates from the local transport dynamics such as the nonlinear friction or the threshold dynamics. The ∇h term is the linear current present in any diffusive process; a_1 can be interpreted as the surface tension for the sandpile. Due to the anisotropy in (b), the surface tension is in general a tensor $\overleftrightarrow{\nu}$, with components $\nu_\parallel$ and $\nu_\perp$ in directions parallel and perpendicular to $\hat{\mathbf{T}}$. We thus arrive at

$$\mathbf{j} = -\nu_\perp\nabla_\perp h - \nu_\parallel\partial_\parallel h\hat{\mathbf{T}} + \frac{\lambda}{2}h^2\hat{\mathbf{T}} , \tag{6}$$

and the equation of motion [Eq. (5)] becomes

$$\partial_t h(\mathbf{x},t) = \nu_\parallel\partial_\parallel^2 h + \nu_\perp\nabla_\perp^2 h - \frac{\lambda}{2}\partial_\parallel(h^2) + \eta(\mathbf{x},t) . \tag{7}$$

Before we present a detailed analysis of Eq. (7), we emphasize that its most important feature is the absence of a relaxation term of the form $-h/\tau$. Such a term introduces a characteristic time τ, and a corresponding length $l = (\tau^2/\nu)^{1/2}$, and destroys scale invariance. It is the conservative nature of the deterministic dynamics that rules out this term in Eq. (7).

Equation (7) is familiar in the context of driven diffusion, and has been studied [31] in the presence of a conservative noise (to be discussed in Sec. III D). In the present case, the addition of sand particles from outside destroys the local conservation rule. Although in steady state the balance of drainage from the boundaries and the flux of the added particles implies $\langle \eta(\mathbf{x},t) \rangle = 0$, the randomness in the deposition process is mimicked by an uncorrelated Gaussian noise with the leading moment

$$\langle \eta(\mathbf{x},t)\eta(\mathbf{x}',t') \rangle = 2D\delta^d(\mathbf{x}-\mathbf{x}')\delta(t-t') , \tag{8}$$

in the hydrodynamic limit. Here D is a measure of the strength of the noise; it is related to the local deposition rate p of Sec. II by $D \propto p^2$. Note that D may be dependent on the box size L due to the size dependences of p and the coarse-graining units l_0 and t_0. Such explicit size dependence (forced upon us by the output limitation of the sandpile automaton) somewhat complicates the essential scaling studies. We shall initially ignore such complications and analyze the scaling behavior of Eqs. (7) and (8). The considerations that lead to these equations are generally valid for dissipative transport in open systems, and may also describe, for example, the flow of current along a wire with random sources and sinks.

B. A dynamical renormalization-group analysis

To study the scaling of fluctuations in the hydrodynamic region, we do a dynamical renormalization-group calculation [13]. We calculate the two-point correlation function $\langle [h(\mathbf{x},t) - h(\mathbf{x}',t')^2 \rangle \equiv C(\mathbf{x}-\mathbf{x}', t-t')$. In the absence of any nonlinearity, Eq. (7) is simply a diffusion equation with anisotropy. Its solution is

$$C(\mathbf{x},t)=\frac{D}{\nu_\parallel}x_\parallel^{2-d}F\left[\frac{\nu_\parallel t}{x_\parallel^2}\left[\frac{\nu_\parallel}{\nu_\perp}\right]^{1/2}\frac{x_\perp}{x_\parallel}\right], \tag{9}$$

where F is a scaling function with usual limiting behaviors, and as usual we have generalized the problem to d dimensions (d is the dimension of the surface, i.e., $d=1$ for the automaton in Sec. II). Nonlinearity can be included perturbatively, and its effect is a modification (i.e., renormalization) of the parameters D, $\nu_\parallel$, and $\nu_\perp$, for example,

$$D^R=D[1+a_1(\lambda x_\parallel^\epsilon)+a_2(\lambda x_\parallel^\epsilon)^2+\cdots], \tag{10}$$

with similar expansions for $\nu_\parallel^R$ and $\nu_\perp^R$. Here $\epsilon=4-d$, and $x_\parallel^\epsilon$ appears by dimensional analysis, so that the combination $\lambda x_\parallel^\epsilon$ is dimensionless. For renormalizable theories, series such as Eq. (10) can be summed to yield scaling forms. The parameters become

$$\begin{aligned}D^R&=D[1+\alpha_1(\lambda x_\parallel^\epsilon)]^{\beta_1},\\ \nu_\parallel^R&=\nu_\parallel[1+\alpha_2(\lambda x_\parallel^\epsilon)]^{\beta_2},\\ \nu_\perp^R&=\nu_\perp[1+\alpha_3(\lambda x_\parallel^\epsilon)]^{\beta_2},\end{aligned}$$

to first order in ϵ. Inserting the above in Eq. (9), we find that in the hydrodynamic limit ($x_\parallel\to\infty$) the correlation function has the simple form

$$C(\mathbf{x},t)\sim x_\parallel^{2\chi}F\left[\frac{t}{x_\parallel^z},\frac{x_\perp}{x_\parallel^\zeta}\right], \tag{11}$$

where the exponents χ, z, and ζ characterize the roughness, dynamic scaling, and anisotropy of the surface, respectively. In the absence of nonlinearity, the "free" diffusion equation yields exponent values $\chi_0=(2-d)/2$, $z_0=2$, and $\zeta_0=1$ from Eqs. (9) and (11). Finding the exponents for the nonlinear equation requires knowledge of the entire perturbation series in Eq. (10). The method of renormalization group shortcuts this process by making the hypothesis [32] that $C(\mathbf{x},t)$ indeed scales as in Eq. (11). Then the series of operations outlined below leads to the exponents χ, z, and ζ.

(i) Naive dimensions. A change of scale $x_\parallel\to bx_\parallel$ is accompanied by $t\to b^z t$, $\mathbf{x}_\perp\to b^\zeta\mathbf{x}_\perp$, and $h\to b^\chi h$. After rescaling, Eq. (7) transforms to

$$\begin{aligned}b^{\chi-z}\frac{\partial h}{\partial t}=&\nu_\parallel b^{\chi-2}\partial_\parallel^2 h+\nu_\perp b^{\chi-2\zeta}\partial_\perp^2 h\\ &-\frac{\lambda}{2}b^{2\chi-1}\partial_\parallel h^2+b^{-z/2-(d-1)\zeta/2-1/2}\eta,\end{aligned}$$

where Eq. (8) is used to determine the scaling of η. Thus the naive scaling for these parameters is

$$\begin{aligned}&\nu_\parallel\to b^{z-2}\nu_\parallel,\\ &\nu_\perp\to b^{z-s\zeta}\nu_\perp,\\ &\lambda\to b^{\chi+z-1}\lambda,\\ &D\to D^{z-2\chi-\zeta(d-1)-1}.\end{aligned} \tag{12}$$

(ii) Perturbative calculation. We next calculate the perturbative corrections to these parameters, to leading order in the nonlinearity. In terms of the Fourier modes

$$h(\mathbf{x},t)=\frac{1}{2\pi}\frac{1}{(2\pi)^d}\int\int d\omega\, d^dk\, h(\mathbf{k},\omega)e^{i(\mathbf{k}\cdot\mathbf{x}-\omega t)},$$

Eq. (7) is

$$h(\mathbf{k},\omega)=G_0(\mathbf{k},\omega)\eta(\mathbf{k},\omega)-\frac{\lambda}{2}G_0(\mathbf{k},\omega)(ik_\parallel)\frac{1}{(2\pi)^d}\frac{1}{2\pi}\int\int d^dq\, d\mu\, h(\mathbf{q},\mu)h(\mathbf{k}-\mathbf{q},\omega-\mu). \tag{13}$$

Here

$$G_0(\mathbf{k},\omega)=\frac{1}{\nu_\parallel k_\parallel^2+\nu_\perp k_\perp^2-i\omega}$$

is the bare propagator, and the Fourier-transformed noise spectrum is

$$\langle\eta(\mathbf{k},\omega)\eta(\mathbf{k}',\omega')\rangle=2D\delta^d(\mathbf{k}+\mathbf{k}')\delta(\omega+\omega'). \tag{14}$$

Equation (13) is a convenient starting point for a perturbative calculation of $h(\mathbf{k},\omega)$ in powers of λ as indicated diagrammatically in Fig. 17. The graphic expansion is quite standard [33,34] with ——→ indicating the propagator G_0, and × depicting the noise $\eta(\mathbf{k},\omega)$. The averaging over stochastic noise is performed using Eq. (14), and the renormalized response function $G(\mathbf{k},\omega)$ [defined by $h(\mathbf{k},\omega)\equiv G^R(\mathbf{k},\omega)\eta(\mathbf{k},\omega)$] is given perturbatively in Fig. 18(a). The lowest-order (one-loop) correction is

$$\begin{aligned}G^R(\mathbf{k},\omega)=G_0(\mathbf{k},\omega)+4\left[\frac{\lambda}{2}\right]^2 2DG_0^2(\mathbf{k},\omega)\frac{1}{2\pi}\frac{1}{(2\pi)^d}\int d\mu\, d^dq ik_\parallel i\left[\frac{k_\parallel}{2}-q_\parallel\right]G_0\left[\frac{\mathbf{k}}{2}-\mathbf{q},\frac{\omega}{2}-\mu\right]G_0\left[\frac{\mathbf{k}}{2}+\mathbf{q},\frac{\omega}{2}+\mu\right]\\ \times G_0\left[-\frac{\mathbf{k}}{2}-\mathbf{q},-\frac{\omega}{2}-\mu\right]+O(\lambda^4),\end{aligned}$$

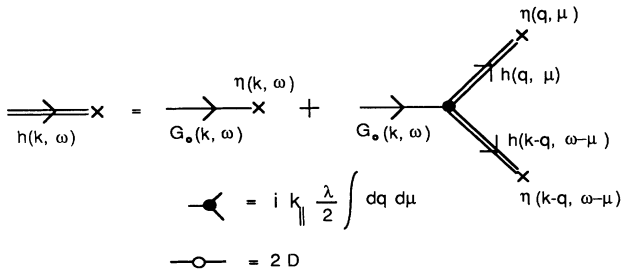

FIG. 17. Diagrammatic representation of the nonlinear integral equation (13) and the perturbation series that results from it.

where the combinatorial factor of 4 represents possible noise contractions leading to Fig. 18(a).

Clearly, the above correction to the propagator is proportional to $k_{\parallel}$. For symmetry reasons odd powers of $k_{\parallel}$ and $k_{\perp}$ cannot survive after the spherical averaging in $\int d^d q$. The leading k dependences are therefore of the form $k_{\parallel}^2$, $k_{\parallel}^4$, and $k_{\parallel}^2 k_{\perp}^2$ of which only the $k_{\parallel}^2$ term is kept since we are interested in the hydrodynamical limit of $k \to 0$. After performing the integrals (see Appendix A), we have to $O(k^2)$,

$$G_0^R(\mathbf{k},0)=G_0(\mathbf{k},0)+G_0^2(\mathbf{k},0)\left[-\frac{3\pi}{32}\nu_{\parallel}k_{\parallel}^2\left[u\frac{k_{\parallel}^{-\epsilon}}{\epsilon}\right]\right], \tag{15}$$

where $\epsilon=4-d$ and we have defined an effective coupling constant

$$u \equiv \frac{\lambda^2 D}{\nu_{\parallel}^{3/2}\nu_{\perp}^{3/2}}\frac{2S_{d-1}}{(2\pi)^d} .$$

The propagator can now be written as

$$G^R(\mathbf{k},0)=\frac{1}{\nu_{\parallel}^R k_{\parallel}^2+\nu_{\perp}^R k_{\perp}^2-i\omega} ,$$

with the effective surface tension

$$\nu_{\parallel}^R=\nu_{\parallel}\left[1+\frac{3\pi}{32}\left[u\frac{k_{\parallel}^{-\epsilon}}{\epsilon}\right]+O(u^2)\right], \tag{16}$$

and $\nu_{\perp}^R=\nu_{\perp}$. Note that there is no correction to $\nu_{\perp}$ to leading order because the nonlinearity is proportional to $k_{\parallel}$. In fact $\nu_{\perp}$ is not renormalized to *any* order of the perturbation expansion because the perturbative corrections are always proportional to $k_{\parallel}$ as shown in Fig. 18(a).

A renormalized noise spectrum $D^R(\mathbf{k},\omega)$ can also be defined from

$$\langle h(-\mathbf{k},-\omega)h(\mathbf{k},\omega)\rangle=2G^R(\mathbf{k},\omega)G^R(-\mathbf{k},-\omega)\times D^R(\mathbf{k},\omega) . \tag{17}$$

Because the vertex is proportional to $k_{\parallel}$, the leading order graph [Fig. 18(b)] is of order $k_{\parallel}^2$ which can again be neglected in the hydrodynamic limit and the coefficient D is not renormalized to all orders in the perturbation series, $D^R=D$.

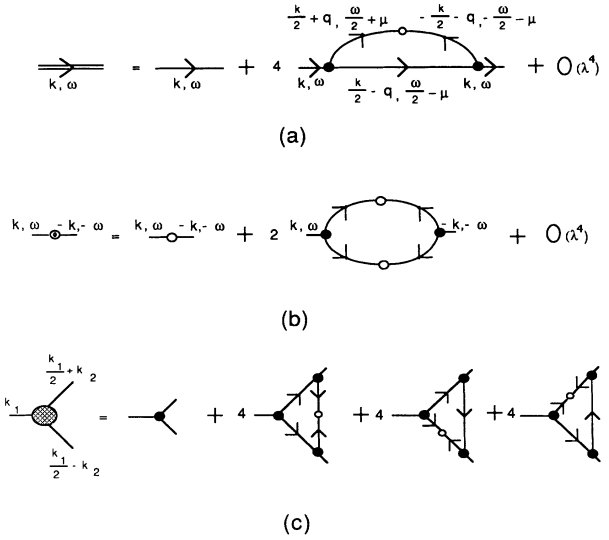

FIG. 18. After averaging over the noise, the perturbation series of Eq. (13) can be reorganized to describe (a) a renormalized propagator, (b) a renormalized noise spectrum, and (c) a renormalized vertex function (or interaction parameter).

The last parameter to consider is the nonlinearity coefficient λ which has a contribution from the graphs in Fig. 18(c). A one-loop calculation gives a null result. In fact this result is also true to all orders of the perturbation series. The nonrenormalizability of λ is due to a Galilean invariance [34] in the equation of motion. Equation (7) is invariant under the reparametrization $x_{\parallel}-x_{\parallel}-\delta\lambda t$, $t \to t$ if $h \to h+\delta$. Note that the parameter λ appears both as the coefficient of the nonlinearity in Eq. (7) and as an invariance factor relating the $x_{\parallel}$ and t reparametrizations. From this symmetry, it follows [33,34] that any renormalization of the driven-diffusion equation that preserves Galilean invariance must leave the coefficient λ unchanged, i.e., $\lambda^R=\lambda$ to all orders.

(iii) Recursion relations. Let us find the rescaling behavior of the surface tension $\nu_{\parallel}$. Define an observation length scale $k_{\parallel}^{-1}=bl_0$ where l_0 is the microscopic cutoff length. Then the dimensionless renormalized surface tension is

$$\tilde{\nu}_{\parallel}^R(b)\equiv\nu_{\parallel}^R(bl_0)^{z-2} =\nu_{\parallel}(bl_0)^{z-2}\left[1+\frac{3\pi}{32}u\frac{(bl_0)^{\epsilon}}{\epsilon}+O(u^2)\right] .$$

We apply the rescaling operator and obtain

$$b\frac{\partial}{\partial b}\tilde{\nu}_{\parallel}^R(b)=\nu_{\parallel}(bl_0)^{z-2}\left[z-2+\frac{3\pi}{32}u(bl_0)^{\epsilon}\right] .$$

We assume the renormalizability of the theory and replace $\nu_{\parallel}$ by $\nu_{\parallel}^R$. Then $\nu_{\parallel}(bl_0)^{z-2}=\tilde{\nu}_{\parallel}^R(b)$, and

$$u(bl_0)^{\epsilon}=\frac{(\lambda^R)^2 D^R}{(\nu_{\parallel}^R)^{3/2}(\nu_{\perp}^R)^{3/2}}\frac{2S_{d-1}}{(2\pi)^d}(bl_0)^{2-d}\equiv\tilde{u}^R(b)$$

(since we already have $\lambda^R=\lambda$, $D^R=D$, $\nu_{\perp}^R=\nu_{\perp}$). Expressing in terms of $l\equiv\ln b$, we arrive at the recursion relation

$$\frac{d}{dl}\tilde{\nu}_{\parallel}^{R}=\tilde{\nu}_{\parallel}^{R}\left[z-2+\frac{3\pi}{32}\tilde{u}^{R}\right], \tag{18}$$

and similarly

$$\frac{d}{dl}\tilde{\nu}_{\perp}^{R}=\tilde{\nu}_{\perp}^{R}(z-2\zeta), \tag{19}$$

$$\frac{d}{dl}\tilde{\lambda}^{R}=\tilde{\lambda}^{R}(\chi z-1). \tag{20}$$

$$\frac{d}{dl}\tilde{D}^{R}=\tilde{D}^{R}[z-2\chi-(d-1)\zeta-1]. \tag{21}$$

(iv) RG flows, fixed points and exponents. In the thermodynamic limit ($b\to\infty$ or $l\to\infty$), we expect the scaling behavior to be described by Eq. (11). If this expectation is true, then the renormalized parameters, such as $\tilde{\nu}^{R}$, should be dimensionless in the hydrodynamic limit. This for example, implies $(d/dl)\tilde{\nu}_{\parallel}^{R}=0$ as $l\to\infty$, and the exponents may be solved at the infrared fixed point ($l\to\infty$) of the flow equations (18)–(21).

Since Eqs. (19)–(21) are correct to all orders, we immediately obtain the *exact* exponents,

$$\chi=\frac{1-d}{7-d},\quad z=\frac{6}{7-d},\quad \zeta=\frac{3}{7-d}. \tag{22}$$

Substituting the above equations in the recursion relation of Eq. (18), we obtain the flow equation for the effective interaction parameter to first order,

$$\frac{d}{dl}\tilde{u}^{R}=\tilde{u}^{R}\left[(4-d)-\frac{9\pi}{64}\tilde{u}^{R}\right]. \tag{23}$$

Above the upper critical dimension of $d_c=4$, the nonlinearity is irrelevant and we recover the ideal scaling with $z_0=2$, $\chi_0=(2-d)/2$, and $\zeta_0=1$. Below $d=4$, there is a stable fixed point at $\tilde{u}^{*}\equiv\tilde{u}^{R}(l\to\infty)=(64/9\pi)\epsilon$ to first order in $\epsilon=4-d$. At the fixed point $\tilde{u}^{*}$, the scaling of the surface is exactly described by the exponents in Eq. (22).

It is important to realize that although the fixed point $\tilde{u}^{*}$ is known only perturbatively to $O(\epsilon)$, the scaling exponents in Eq. (22) are exact as long as the parameters $\nu_{\perp}$, D, and λ are finite. The exactness of these exponents follows from the nonrenormalizability conditions on $\nu_{\perp}$, λ, and D which remove anomalous dimensions to all orders. This point can be illustrated by a direct examination of the correlation function $C(\mathbf{x},t)$. We have already shown that the parameters D, λ, and $\nu_{\perp}$ are not changed by the inclusion of nonlinearity. The form of $\nu_{\parallel}^{R}$ can be obtained from integration of the flow equation. From Eq. (23) we obtain the renormalized coupling constant:

$$\tilde{u}^{R}(x_{\parallel})=\frac{ux_{\parallel}^{\epsilon}}{1+(9\pi/64)(u/\epsilon)x_{\parallel}^{\epsilon}}\quad\text{with } x_{\parallel}=l_0e^{l}$$

to leading order in ϵ. The renormalized surface tension is now obtained by integrating Eq. (18) as

$$\tilde{\nu}_{\parallel}^{R}(x_{\parallel})=\nu_{\parallel}^{R}x_{\parallel}^{z-2}=\nu_{\parallel}x_{\parallel}^{z-2}=\nu_{\parallel}x_{\parallel}^{z-2}\left[1+\frac{9\pi}{64}\frac{u}{\epsilon}x_{\parallel}^{\epsilon}\right]^{1/3}.$$

Inserting $\nu_{\parallel}^{R}(x_{\parallel})$, $D^{R}=D$, $\lambda^{R}=\lambda$, and $\nu_{\perp}^{R}=\nu_{\perp}$ into Eq. (11) results in the renormalized correlation function

$$C^{R}(\mathbf{x},t)=\frac{D}{\nu_{\parallel}}\left[1+\frac{9\pi}{64}\frac{u}{\epsilon}x_{\parallel}^{\epsilon}\right]^{-1/3}x_{\parallel}^{2-d}F\left(\frac{\nu_{\parallel}t}{x_{\parallel}^{2}}\left[1+\frac{9\pi}{64}\frac{u}{\epsilon}x_{\parallel}^{\epsilon}\right]^{1/3},\left[\frac{\nu_{\parallel}}{\nu_{\perp}}\right]^{1/2}\frac{x_{\perp}}{x_{\parallel}}\left[1+\frac{9\pi}{64}\frac{u}{\epsilon}x_{\parallel}^{\epsilon}\right]^{1/6}\right). \tag{24}$$

Comparing the above with Eq. (11), we immediately regain the exponents of Eq. (22) in the hydrodynamic limit $x_{\parallel}\to\infty$. It is now apparent that the higher loop corrections will only change the coefficient in front of $x_{\parallel}^{\epsilon}$ (i.e., the fixed point value and the detailed shape of the scaling function F) but not the exponents themselves. It is also worth noting that the diagrams which contribute to order $k_{\parallel}^{2}k_{\perp}^{2}$ in the propagator $G^{R}(\mathbf{k},\omega)$ and to order $k_{\parallel}^{2}$ in the noise spectrum $D^{R}(\mathbf{k},\omega)$ also amount to a correction to the coefficient of $x_{\parallel}^{\epsilon}$ and do not modify the leading scaling behaviors of Eq. (22).

Finally we point out that the roughening exponent χ as given by Eq. (22) is negative for $d>1$. Since the width of the interface is characterized by $\omega\sim L_{\parallel}^{\chi}$, then $\chi<0$ implies that the surface is asymptotically *flat* for $d>1$. This provides a self-consistent check of the "flat surface" assumption made at the beginning of this analysis. The assumption is no longer valid below $1+1$ dimensions.

C. Scaling of fluctuations

The exponents χ, z, and ζ are the fundamental scaling dimensions of the system; other quantities can in principle be calculated from them. In particular, we are interested in the spatial and temporal correlations of observables such as the transport current and the rate of energy dissipation. In the following, we show how the spatial and temporal fluctuations can be related to the fundamental dynamical field h.

1. Spatial structures

To probe the spatial structure of our fluctuating surface, we need to calculate its response to an infinitesimal perturbation as follows. We start with some initial height configuration $h_0(\mathbf{x})$, add particles randomly as described by $\eta(\mathbf{x},t)$, and obtain a series of height profiles $h(\mathbf{x},t)$. This is followed by another run starting from the same configuration $h_0(\mathbf{x})$, and adding particles with the same randomness $\eta(\mathbf{x},t)$ except for a small difference $\delta\eta(\mathbf{x},t)$. The surface profile obtained the second time is $h'(\mathbf{x},t)$ and is different from the first by an amount $\delta h(\mathbf{x},t)=h(\mathbf{x},t)-h'(\mathbf{x},t)$. The response function is now defined by $\delta h(\mathbf{x},t)=\int d\mathbf{x}'dt'R(\mathbf{x},\mathbf{x}',t,t')\delta\eta(\mathbf{x}',t')$, and can be calculated by substituting $h+\delta h$ for h and $\eta+\delta\eta$ for η in Eq. (7),

$$\frac{\partial}{\partial t}(\delta h)=\nu_{\parallel}\partial_{\parallel}^2(\delta h)+\nu_{\perp}\nabla_{\perp}^2(\delta h)-\lambda\partial_{\parallel}(h\,\delta h)$$
$$-\frac{\lambda}{2}\partial_{\parallel}(\delta h)^2+\delta\eta\ .$$

To linear order, the response function is represented by the following shorthand:

$$R(\mathbf{x},t)=\left[\frac{\partial}{\partial t}-\nu_{\parallel}\partial_{\parallel}^2-\nu_{\perp}\nabla_{\perp}^2+\lambda\partial_{\parallel}h+\lambda h\partial_{\parallel}\right]^{-1}\ . \quad (25)$$

In Fourier space the linear response function with $\lambda=0$ is the free propagator $R_0(\mathbf{k},\omega)=1/(-i\omega+\nu_{\parallel}k_{\parallel}^2+\nu_{\perp}k_{\perp}^2)$. With $\lambda\neq 0$, since $z<2$ as found in the preceding section, the term $\lambda\partial_{\parallel}h\sim x_{\parallel}^{\chi-1}=x_{\parallel}^{-z}$ in Eq. (25) dominates over the $\partial_{\parallel}^2$ term in the hydrodynamic limit. The large-distance scaling properties are therefore governed by

$$R(\mathbf{k},\omega)=\frac{1}{\omega}f\left[\frac{\omega}{k_{\perp}^2},\frac{\omega}{k_{\parallel}^z}\right]\ .$$

For a point perturbation $\delta\eta(\mathbf{x},t)=\delta(t)\delta^d(\mathbf{x})$, the response scales as

$$\delta h(\mathbf{x},t)=t^{-d/z}f\left[\frac{t}{x_{\perp}^2},\frac{t}{x_{\parallel}^z}\right]\ . \quad (26)$$

Note that the above result is another expression of the conservation condition. Not surprisingly, the influence of the perturbation spreads as $t^{1/2}$ perpendicular to the driving direction and as $t^{1/z}>t^{1/2}$ in the downhill direction. In $2+1$ dimensions $1/z=5/6$, and the effect of anisotropy is quite dominating. (This is the reason for choosing narrow strip geometries in the simulation of 2D sandpiles in Sec. II B.) From Eq. (26), we can also calculate the size distribution of the sites influenced, the fractal dimension of the influenced region, etc. However, the relation of these quantities to the fundamental dynamical field h is model dependent and will not be pursued here. As mentioned in the Introduction, transport systems such as the sandpile automata are more suited for the study of temporal fluctuations which we turn to next.

2. *Temporal fluctuations*

To make comparison with the simulation results of previous sections possible, we compute the power spectra for the output current $J(t)$ and the energy dissipation $E(t)$. Obtaining the scaling behaviors of these *global* quantities is often not as straightforward as it naively appears. Here we shall only sketch the result by using naive scaling analysis. A careful derivation is carried out in Appendix B. The output current measured in Sec. II is the integrated local current $\mathbf{j}(\mathbf{x},t)$ at the boundary $x_{\parallel}=L_{\parallel}$, i.e., $J(t)=\int d^{d-1}x_{\perp}\mathbf{j}(L_{\parallel},\mathbf{x}_{\perp},t)\cdot\hat{\mathbf{T}}$ for a general $(d+1)$-dimensional system. Using Eq. (6) for $\mathbf{j}$ and noting that in $d<4$ scaling is dominated by the h^2 part of the current, we obtain

$$\langle J(t)J(0)\rangle_c=\int_{L_{\perp}}d^{d-1}x_{\perp}d^{d-1}x_{\perp}'\langle h^2(\mathbf{x},t)h^2(\mathbf{x}',0)\rangle_c$$
$$\sim L_{\perp}^{d-1}t^{[4\chi+(d-1)\zeta]/z}\ ,$$

where we have used $\langle h^2(\mathbf{x},t)h^2(\mathbf{0},0)\rangle_c \sim\langle h(\mathbf{x},t)h(\mathbf{0},0)\rangle_c^2$. (The subscript c denotes the cumulant or connected part of the correlation function, i.e., measures fluctuations around the average.) The Fourier transform of the above correlation function yields the power spectrum

$$S_J(\omega)\sim L_{\perp}^{d-1}\omega^{-\alpha_J}\ , \quad (27)$$

with $\alpha_J=1/z$.

A similar calculation is carried out for the rate of energy dissipation $E(t)$. Here we start from the total "potential energy" of the system, $U(t)=\frac{1}{2}\int d^dx[\tilde{H}(\mathbf{x},t)]^2$, where $\tilde{H}(\mathbf{x},t)=H_0(\mathbf{x})+h(\mathbf{x},t)$ is the time-dependent coarse-grained landscape of the sandpile. The energy dissipation rate is simply obtained from the loss of potential energy, i.e.,

$$E(t)=-\frac{dU}{dt}=-\int d^dxH_0(\mathbf{x})\frac{\partial h}{\partial t}\ ,$$

where only the leading order term in $h(\mathbf{x},t)$ is kept. Using the equation of motion, Eq. (7), and integrating by parts, we obtain

$$E(t)=\int d^dx\hat{\mathbf{T}}\cdot\mathbf{j}(\mathbf{x},t)=\int d^dxh^2(\mathbf{x},t)\ . \quad (28)$$

We see that the total energy dissipated at each time is just the sum of local transport activities, precisely the quantity monitored in the simulation. The energy correlation function is again calculated using the basic correlation function $\langle hh\rangle$, giving

$$\langle E(t)E(0)\rangle_c=\int d^dxd^dx'\langle h^2(\mathbf{x},t)h^2(\mathbf{x}',0)\rangle_c$$
$$\sim L^dt^{[4\chi+(d-1)\zeta+1]/z}\ .$$

Fourier transforming the above then yields the power spectrum for energy dissipation,

$$S_E(\omega)\sim L^d\omega^{-\alpha_E}\ , \quad (29)$$

with $\alpha_E=2/z$.

In the above calculations, simplifying assumptions regarding the form of the correlation function $\langle h^2h^2\rangle$ were implicitly used. We explore more general scaling forms in Appendix B and find that $1/z<\alpha_E\leq 2/z$, while $\alpha_J=1/z$ is not affected. The numerical values of these exponents in various substrate dimensions are listed in Table II. For comparison, we have also listed in Table II

TABLE II. Numerical values of exponents obtained by using the dynamical renormalization-group method. Also included are exponents $\alpha^{(0)}$ obtained from the linear theory.

d	4	3	2	1
z	2	$\frac{3}{2}$	$\frac{6}{5}$	1
χ	-1	$-\frac{1}{2}$	$-\frac{1}{5}$	0
ζ	1	$\frac{3}{4}$	$\frac{3}{5}$	
α_J	$\frac{1}{2}$	$\frac{2}{3}$	$\frac{5}{6}$	1
α_E	$\frac{1}{2}$–1	$\frac{2}{3}$–$\frac{4}{3}$	$\frac{5}{6}$–$\frac{5}{3}$	1–2
$\alpha_J^{(0)}$	$\frac{1}{2}$	$\frac{1}{2}$	$\frac{1}{2}$	$\frac{1}{2}$
$\alpha_E^{(0)}$	2	2	2	$\frac{3}{2}$

the exponents $\alpha_J^{(0)}$ and $\alpha_E^{(0)}$ that result from the linear diffusion equation where ∇h is used as the local current j (see Appendix B). An earlier investigation of $1/f^{\alpha}$ noise in linear diffusive systems can be found in Ref. [35].

3. *Comparison to simulations*

From Table II we see that the exponent $\alpha_J = 1$ in $d = 1$ agrees with the numerical simulations of Sec. II. But a direct comparison of the exponent α_E has not been possible, although the observed α_E is at the edge of the allowed values according to Appendix B. We also observe that the exponents of the linear equation in Table II are not applicable to α_E or α_J. It is surprising that similar values are found numerically for the two exponents, since J is a measure of surface fluctuations while E is a measure of bulk fluctuations. This suggests a strong correlation between fluctuations in the bulk and at the surface. One possible explanation is that the size dependence of the microscopic cutoff (i.e., $l_0 \sim L^{1/2}$) in the numerical model drastically reduces the effective size of the system. It forces the various parameters appearing in the equation of motion, Eq. (7), to be L dependent. This in turn may cause anomalous scaling of spatially averaged quantities (see Appendix B) and hence the anomalous power spectrum for global energy dissipation. Also, this would modify the L dependences of the power spectra, making a direct comparison to theory difficult.

Carlson *et al.* [36] have also looked for a diffusion equation to describe transport in sandpile automata in the single-avalanche region. For a variant of the model (the two-state model), they found that the hydrodynamic behavior is described by a diffusion equation with a singular diffusion coefficient. They also provide numerical evidence suggesting that the 1D sandpile automaton investigated here may be described by singular diffusion. Does this singularity reflect the anomalous size dependence of "microscopic"' parameters discussed above, or is it a reflection of the breakdown of the linear diffusion equation due to relevance of nonlinearities (since $z < 2$ the nonlinear equation clearly exhibits superdiffusive behavior)? We have not succeeded in making a clear correspondence to this work. As analysis in this section indicates, the behaviors of the sandpile automaton (in the interacting avalanche region) are at least consistent with the expectations of a noisy driven-diffusion system. However, the task of constructing a definitive macroscopic equation to describe each region of the sandpile automaton remains incomplete.

IV. GENERIC SCALE INVARIANCE

A. Origin of scale invariance

In this section we shall attempt to formulate a general approach to open and *extended* dynamical systems exhibiting scale-invariant fluctuations. As many deterministic dynamical systems with few degrees of freedom are known to exhibit nontrivial chaotic behavior, it is important to emphasize the infinitely many degrees of freedom in extended systems. The successful statistical approach to near equilibrium critical phenomena [5] demonstrates that when correlations extend over large spatial intervals details of the interactions at short distances become irrelevant. It is thus appropriate to apply a coarse graining to eliminate such details, and to focus on averaged behavior. Let us assume that after such averaging fluctuations in the system of interest are described by a field $h(\mathbf{x},t)$, e.g., giving the height of an evolving "sandpile" around some equilibrium configuration. We now outline the reasoning that leads to constructing an equation of motion for $h(\mathbf{x},t)$ [37].

Over sufficiently long time scales, inertial terms (e.g., $\partial_t^2 h$) are irrelevant in the presence of dissipative dynamics, and hence the evolution of h is governed by

$$\partial_t h = F[h] + \eta(\mathbf{x},t) \ . \tag{30}$$

For systems evolving according to a Hamiltonian $\mathcal{H}[h]$, the deterministic force F can be obtained from the derivatives of $\mathcal{H}$, and the stochastic noise $\eta(\mathbf{x},t)$ is related to thermal fluctuations [13]. However, for an open system undergoing an irreversible evolution, there is no apparent $\mathcal{H}[h]$, and finding $F[h]$ is nontrivial. In analogy to the Landau theory of phase transitions, it is reasonable to expect that all terms compatible with symmetries and conservation laws should be present in the equation of motion.

Apart from a trivial constant, the first term in a *local* expansion of $F[h]$ is $-h/\tau$. (Since, by fiat, we consider small fluctuations around a stable state, the sign of the linear term has to be negative.) Such a contribution clearly introduces a time scale τ in the problem and destroys any self-similarity of temporal fluctuations. One mechanism for getting rid of such a term is to tune an external parameter until $1/\tau$ accidentally vanishes: this is clearly externally imposed and incompatible with the idea of SOC. A second mechanism is the one used in Sec. III B, where we pointed out that in the sandpile simulations the quantity $\int d^d\mathbf{x} h(\mathbf{x},t)$ is conserved during the deterministic evolution. Such a conservation law is not compatible with a linear term in the expansion, and thus quite naturally removes the time scale τ. Actually, even a conservation law is not necessary: A third mechanism that removes $-h/\tau$ is a translational symmetry in h. If the system is invariant under the transformation $h(\mathbf{x}) \to h(\mathbf{x}) + h_0$, then again there will be no characteristic time scale. This last mechanism accounts for the self-similarity of models of interface dynamics [8,34].

We have thus established that symmetries or conservation laws can naturally eliminate the time scale τ, and lead to self-similar temporal fluctuations without any tuning. However, as pointed out by Grinstein, Sachdev, and Lee [38], the absence of a *time* scale does not necessarily imply the existence of self-similar correlations in *space*. The linear diffusion equation with conserved noise and the Ising model with conserved magnetization provide clear examples. Both problems take the standard Langevin form

$$\partial_t h = \nabla^2 \left[\frac{\partial \mathcal{H}}{\partial h} \right] + \nabla \eta(\mathbf{x},t) \ ,$$

for conservative dynamics [13]. With $\langle \eta(\mathbf{x},t)\eta(\mathbf{x}',t')\rangle = \delta^d(\mathbf{x}-\mathbf{x}')\delta(t-t')$, the spatial correlations are governed by the steady-state distribution $\mathcal{P}[h]\sim\exp[-\mathcal{H}]$. Since a generic $\mathcal{H}$ will not be at its critical point, the steady-state correlations in space will not be self-similar, but characterized by a correlation length. The temporal correlations still decay algebraically; e.g., for the Navier-Stokes equation the velocity-velocity correlations have the well-known $t^{-d/2}$ tail [33]. It seems appropriate to also exclude these situations from SOC phenomena as the coupling of spatial and temporal self-similarity was one of the original motivations [6]. Actually it has been shown [38,39] that anisotropy or other mechanisms that destroy detailed balance may be sufficient to render the spatial correlations also self-similar. In view of the above, we note that our original statement [29] that "a conservation law is both necessary and sufficient for SOC," which was formulated within the context of sandpiles, is not always valid in a more general framework.

A novel feature of Eq. (30) is that while $F[h]$ may be conservative, the noise η need not be. Such a condition leads to a new class of equations, outside the classification of models A (both F and η nonconservative) and B (both F and η conservative) of Hohenberg and Halperin [13]. Are such equations internally self-consistent, or will the nonconservative noise generate a nonconservative term in F under renormalization? Perturbative analysis, as in Sec. III B, indicates that as all nonlinearities in F originate from $\nabla\cdot\mathbf{J}$, all terms generated by RG will be proportional to ∇^2 and hence conservative. Another consequence of this statement is that the nonconservative noise itself will not be renormalized under RG. As demonstrated in Sec. III B such nonrenormalization always leads to an *exponent identity* for this class of equations. More recently such equations have been proposed for interface growth in which the adsorbed particles undergo conservative rearrangements on the surface [40,41]. Not surprisingly such an exponent identity is recovered for these systems [42]. An earlier example is found in the study of Burgers equation with nonconservative noise by Forster, Nelson, and Stephen [33]. Thus, in this formulation, SOC appears as a characteristic of the deterministic dynamics (F) of the system, independent of the external driving force η.

B. Some other universality classes of transport

We now return to some other transport processes with generic scale invariance. In Sec. III A, we constructed a model describing transport processes that (a) are locally conservative, (b) have a unique transport direction, (c) have a nonconservative uncorrelated noise in the bulk, and (d) have a uniform and stationary gradient set up by the material transported (e.g., flat average surfaces). Given the above conditions, the large-distance, long-time scaling behavior found in Sec. III B is universal, i.e., the "hydrodynamic" properties should not depend on the microscopic details of the system. However, alterations in any of the above conditions can lead to different scaling behaviors; indeed it can even destroy criticality.

Of the four conditions listed above, (d) is by far the least general; its existence was postulated based on simulation results. Also, several other investigations of SOC have focused on models where one or more of the above conditions is clearly not satisfied. To show that these differences can indeed lead to different universality classes, here we shall construct their corresponding continuum theories. We will focus our discuss on conditions (a)–(c) assuming that (d) is somehow satisfied. For systems that do possess an intrinsic time scale in the motion of the gradient, the following discussion only applies up to that time scale during which (d) is still valid.

1. *Local violations of conservation laws*

The importance of the local conservation law has been tested directly in the simulations of Manna, Kiss, and Kertész [43]. They found cutoffs in the distribution functions once the conservation rule was broken by choosing a transfer ratio different from unity. However, they also noted that there are no cutoffs in the simulations if the transfer ratio is allowed to fluctuate around unity. In a continuum formulation of such a model, the stochastic breaking of conservation law can be modeled by a fluctuating mass term, i.e., by $\zeta(\mathbf{x},t)h$, where $\zeta(\mathbf{x},t)$ is a random variable of zero mean. It is easy to verify that as long as $\chi<0$, such terms are irrelevant and do not change the hydrodynamic behavior. In fact, the numerical simulations [43] do indicate a change of scaling of the avalanche distributions with and without such local fluctuations. However, these scaling functions refer to region I of Sec. II B, where the hydrodynamic analysis is not applicable. An important point is that such stochastic violations of the conservation law play the same role as the random external addition of sand, and do not destroy scale invariance.

2. *Variations in noise*

Restricting ourselves to anisotropic transport processes, there are a number of possible variations to the external input of noise. As shown in Sec. III B, the simplest nontrivial equation of motion is

$$\frac{\partial h}{\partial t}=\nu\nabla^2 h-\frac{\lambda}{2}\partial_{\parallel}(h^2)+\eta(\mathbf{x},t)\ . \tag{31}$$

If the noise is *conservative*, i.e.,

$$\langle \eta(\mathbf{x},t)\eta(\mathbf{0},0)\rangle = 2D\nabla^2\delta^d(\mathbf{x})\delta(t)\ , \tag{32}$$

then a change in scale $x\to bx$ (accompanied by $t\to b^z t, h\to b^\chi h$) leads to the following transformation of the parameters:

$$\nu\to b^{z-2}\nu,\quad D\to b^{z-2\chi-d-2}D,\quad \lambda\to b^{\chi+z-1}\lambda\ .$$

In the absence of nonlinearity (i.e., $\lambda=0$), the equation is made scale invariant upon the choice of $z_0=2$ and $\chi_0=-d/2$. A nonlinearity added to this scale-invariant equation has a dimension $y_\lambda^0=\chi_0+z_0-1=1-d/2$. For $d>2$, a small nonlinearity is irrelevant, while below the upper critical dimension of $d_c=2$, it is relevant and grows under rescaling. This is actually the problem of forced particle diffusion studied by Janssen and

Schmittmann [31]. The exponents found are similar to those in Eq. (22) but with d replaced by $d-2$.

In another class of driven transport systems the input is not from the "top" of the box, but from the edge opposite to the open (exit) end. In the simplest scenario, such a process is described by Eq. (31), with a noise spectrum

$$\langle \eta(\mathbf{x},t)\eta(\mathbf{x}',t')\rangle = 2D\delta(x_\parallel)\delta(x'_\parallel)\delta^{d-1}(\mathbf{x}_\perp-\mathbf{x}'_\perp)\delta(t-t') ,$$

where the delta functions $\delta(x_\parallel)\delta(x'_\parallel)$ ensure that noise acts as a source only along the input edge. In the naive scaling analysis the parameters transform as

$$\nu\to b^{z-2}\nu, \quad D\to b^{z-2\chi-d-1}D, \quad \lambda\to b^{\chi+z-1}\lambda .$$

The free exponents (for $\lambda=0$) are in this case $z_0=2$, $\chi_0=1-d/2$, giving the nonlinearity a dimension $y_\lambda^0=\chi_0+z_0-1==(3-d)/2$, and hence an upper critical dimension of $d_c=3$. This agrees with the upper critical dimension found by Dhar and Ramaswamy [25] for a similar model with input along an edge.

A somewhat different example involving noise from the boundary is provided by the transport of vortices through a piece of type-II superconductor [44]. Recently, this problem was studied numerically by a simple lattice-gas simulation [45]. Instead of a noisy input current at the boundary, the stochasticity in this problem arises from the fluctuation of the density field itself at the boundary. It can also be analyzed in the spirit of the continuum field theory [46] and an upper critical dimension of $d_c=1$ is found. It can be shown that the fluctuation in the total number of vortices in the sample is always $1/f$. Yet another example is provided by sliding charge-density waves.

So far, a noise term was used to mimic the fluctuations in external inputs. But there are also situations in which the stochasticity is generated by the deterministic dynamics itself. One example that bears resemblance to the sandpile problem considered in Sec. III is that of water running down an inclined plane. When the inclination angle is small, water flows smoothly. But if the inclination becomes too steep (i.e., exceeding a threshold), the flow becomes stochastic [47]. For small fluctuations in the thickness of water layer $h(x,t)$, one obtains the following *deterministic* equation of motion:

$$\partial_t h = -\nu_1\partial_x^2 h - \nu_2\partial_x^4 h - \lambda\partial_x(h^2) . \tag{33}$$

Equation (33) is known as the Kuramoto-Sivashinsky (KS) equation [48]. It is derived in this case simply from the Navier-Stokes equation with the proper boundary conditions. Since the KS equation is linearly unstable for long-wavelength modes (negative surface tension), randomness in initial conditions is amplified, resulting in the stochastic behavior of water flow in the hydrodynamic limit. Zalesky [49] further shows that the stochastic behavior exhibited by the KS equation is actually consistent with the Langevin equation (31) with a conservative noise as in Eq. (32). Given that the dynamics is stochastic, Eq. (31) is of course the simplest equation consistent with the symmetry and conservation law requirements of the water flow problem (since they are the same as those for the sandpile problem considered). However, because there is no external source (of water) in the problem, the internally generated noise can at most be conservative as described by Eq. (32).

3. *Quenched randomness*

Another recurring situation is that the medium through which a transport process takes place has quenched randomness. Such a process is described by a "noise" of the form

$$\langle \eta(\mathbf{x},t)\eta(\mathbf{x}',t')\rangle = 2D\delta^d(\mathbf{x}-\mathbf{x}') ,$$

which is explicitly time independent. Similar scaling analysis yields $y_\lambda^0=(6-d)/2$ giving an upper critical dimension $d_c=6$ for this process. In general, for spatially and temporally correlated noise of the form [34]

$$\langle \eta(\mathbf{x},t)\eta(\mathbf{0},0)\rangle \sim |\mathbf{x}|^{2\rho-d}|t|^{2\theta-1} ,$$

the upper critical dimension for the nonlinearity in Eq. (31) is $d_c=4+2\rho+4\theta$.

For models of discretized sand units [30], Toner [50] has included a quenched disordered term appearing as $\cos[Gh+\phi(\mathbf{x},h)]$ in the current, and finds that such disorder removes the roughening transition, always resulting in a rough interface.

4. *The effect of isotropy*

Transport systems do not always have to be driven in one specific direction. As an example, consider the traffic problem in a big city: Assume that the total number of cars on the road is on average constant, but let there be random local sources and sinks (e.g., parking lots). The equation of motion is again given by Eq. (5), where h is now the density of cars and η describes the randomness. What is the form of $\mathbf{j}$ if the cars wander aimlessly? Since the problem is now isotropic, the current operator $\mathbf{j}$ can only be constructed from combinations of ∇ and h's. Leading terms are $\mathbf{j}=-\nu\nabla h+(\lambda/2)\nabla(h^2)$. The first term represents random wanderings of cars (diffusive movement). The second term mimics a cooperative crowding effect. If we write the above current as

$$\mathbf{j}=-\nu\left[1-\frac{\lambda}{\nu}h\right]\nabla h ,$$

it becomes apparent that the second term slows down the wandering of cars if local car density becomes high, i.e., it is more difficult for cars in traffic jams to get out. Inserting the current operator into the conservation law in Eq. (5), we obtain

$$\frac{\partial h}{\partial t}=\nu\nabla^2 h-\frac{\lambda}{2}\nabla^2(h^2)+\eta(\mathbf{x},t) . \tag{34}$$

This is yet another nonlinear diffusion equation. It looks somewhat like the equation that describes the evolution of growing interfaces [8], but is in fact quite different because it does not have the symmetry $h\to h+\text{const}$. Naive dimensional analysis gives an upper critical dimension of 2 above which small nonlinearity is irrelevant. As mentioned in Sec. III D, there is an exponent identity

$z-2\chi=d$ due to nonrenormalization of a nonconservative noise spectrum $\langle \eta(\mathbf{x},t)\eta(\mathbf{0},0)\rangle = 2D\delta^d(\mathbf{x})\delta(t)$. However, the parameters ν and λ do get renormalized and the problem becomes quite complicated. Equation (34) can also be coupled to different types of noise spectra as in the preceding section, leading to new universality classes.

V. CONCLUSIONS

Since its introduction, self-organized criticality (SOC) has captured the imagination of many physicists, and led to an explosion of activity and publications. In this paper we have only referred to a small fraction of these studies which have more closely corresponded to our line of investigation. The common elements in most such studies include a weak external perturbation, a dynamical evolution process, and an eventual response that can be fitted to a power law. The diversity of systems studied makes a quantitative comparison impossible. We shall instead discuss some possible qualitative similarities in a number of such systems.

The majority of studies of SOC have involved numerical simulations of simple cellular automata. There are fewer experimental studies; the clearest examples appear in magnetic domains [51,52]. Experiments have also been conducted on the flow of sand under a variety of conditions: uniform addition to a drum [12], rotating a closed container [53], grain-by-grain addition to an evolving sandpile [54]. This last situation most closely mimics the cellular automaton simulations: while smaller avalanches form a self-similar distribution, there is a cutoff set by large events involving the displacement of the whole top layer. As discussed in Sec. II C, this behavior is somewhat similar to the discharge events observed in the simulations. However, the actual situation is probably more complicated as it involves inertial effects, flow of sand in the bulk, etc. These experiments have resulted in a look at the problems of flow in granular media. A variety of formulations have studied the instabilities [55,56] and phase transitions (segregation of different size grains) [57] in such granular flows.

Possible applications of SOC to earthquakes have also attracted considerable attention [11,58–62]. Seismic data indicate that the distribution of earthquakes versus their energy release indeed follows a power law for at least a large portion of the observed earthquake magnitudes [63]. Models of earthquakes usually start with a network of masses connected by springs (representing one plate in a fault), and subject to nonlinear friction forces. One issue of debate is whether to model the instabilities of a single fault, or the evolution of faults with time. For a single fault there is an excess of large earthquakes, which like the discharge events of the sandpile reset the configuration of the whole system. Such system-wide events thus appear to be a characteristic feature of many systems with threshold instabilities.

There has also been some progress in obtaining exact results pertaining to sandpile automata. Dhar and collaborators have obtained several exact results regarding the number of states, their evolutions, and distribution functions in simple automata [25,26,64]. Carlson *et al.* have focused on the behavior of trapping sites [19] (the stopping points for avalanches), and have also obtained singular diffusion equations for transport [36]. More results along these lines have been reported by Kadanoff *et al.* [65]. These results all pertain to the single-avalanche region described in Sec. II B, which is perhaps the most striking aspect of SOC.

There is emerging consensus that simple superposition of single-avalanche signals will not lead to $1/f$ noise [20,21,66], one of the initial motivations of SOC. However, as we demonstrated in Sec. II B, at finite driving force the avalanches overlap, and the resulting output signals can exhibit $1/f$ noise. Also, due to their overlap, in this regime it is no longer possible to identify single avalanches. We suggest in Sec. III that a continuum "hydrodynamics" description may be appropriate to this region. The idea that such noisy diffusion processes may be responsible for $1/f$ noise is not new [35]. As these ideas could not quantitatively account for the magnitude of such noise, for example in metals, they were abandoned in favor of other explanations, such as activated processes. It is only more recently noted that such diffusionlike equations quite generically result in scale-invariant spatial fluctuations [29,38,39]. Conversely, while the spatial correlations in systems with continuous symmetry have been known for a while, more recently a number of authors have studied $1/f^{\alpha}$ noise in such a system (a growing interface [67,68]).

In the approach of Sec. III, the system acts as a complex filter. White noise is used as an input to the system, while the output current is found to be correlated. (Also snapshots of the system will indicate the presence of spatial correlations.) More recently, Bak has emphasized that *SOC may be present in the absence of any stochastic input;* the example used in a sandpile that is very slowly tilted [60]. In this case the input is a very small dc current, as opposed to white noise. In a continuum formulation instabilities are then necessary to magnify the small dc input. The situation is thus quite similar to the Kuramoto-Sviashinsky equation described in Sec. IV B. It also bears some resemblance to turbulence in the inertial regime: In a uniform flow instabilities originating from the boundaries continue to produce self-similar correlations over an intermediate range of wavelengths. However, there is a crucial difference between turbulence and the cellular automaton Bak *et al.* introduced as the latter requires an infinitesimally small driving force.

But even a small (but finite) dc input will eventually lead to an overlap of avalanches in a large enough system. If we insist upon distinct individual events that follow a self-similar distribution as the main signature of SOC, we must limit to small systems, or scale the noise appropriately, as in Sec. II A. Detailed analytical computations of the distribution functions in this single-avalanche regime are indeed difficult, but can one at least identify the underlying principle of scale invariance? We argued in Sec. IV A that symmetries or conservation laws were responsible for the lack of time scales in the problem. Is it possible that the single-avalanche regime is governed by some other principle, and that the very requirement of distinct events leads to SOC? In the approach of Sec. III, this seems unlikely, as the presence or

absence of the stochasticity cannot account for the lack of characteristic scales. However, Bak, Chen, and Creutz have claimed that such arguments may not be applicable [69]. They provide the "game of life" as a counterexample that shows self-similar scaling in the absence of any apparent conservation laws. But, later simulations on larger systems indicate the presence of a large cutoff length for scale invariance [70]. More recently, Feder and Feder [66] studied another variant of the sandpile automaton in which the conservation law was weakly broken. They did not observe any apparent cutoff in the scaling of avalanche sizes. Are the again limited by the finite-size effect as in the game of life? More extensive simulations are certainly needed here before drawing any conclusions.

Further work can indeed establish whether or not conservation laws and symmetries can account for all situations in which scale invariance is observed. Regardless, even the simple sandpile cellular automaton exhibits a variety of scaling behaviors that challenge our understanding. Indeed this very variety, and range of possible modifications, makes the problem complicated to attack. Further progress may require a more narrow and specific definition of SOC, and the particular behavior that needs to be described for the sandpile.

ACKNOWLEDGMENTS

We would like to thank P. Bak for initiating our interest in this problem. We also benefited from a number of discussions with J. Carlson, G. Grinstein, S. Obukhov, and C. Tang. This research was supported by the National Science Foundation through the MIT Center for Materials Science Grant No. DMR-90-01519 and through Grant No. DMR-90-96267, further NSF support, and by IBM. M.K. acknowledges support from the A. P. Sloan Foundation.

APPENDIX A: PROPAGATOR RENORMALIZATION

The first-order correction to $G^R(\mathbf{k},\omega)$ is $G_0^2(\mathbf{k},\omega)\Sigma(\mathbf{k},\omega)$ where Σ is calculated from the diagram in Fig. 18(a), as

$$\Sigma(\mathbf{k},\omega)=4\left[\frac{\lambda}{2}\right]^2 2D\frac{1}{(2\pi)^d}\frac{1}{2\pi}\int\int d^dq\,d\mu\,\frac{ik_\parallel i(k_\parallel 2-q_\parallel)}{\nu_\parallel(k_\parallel/2-q_\parallel)^2+\nu_\perp(k_\perp/2-q_\perp)^2-i(\omega/2-\mu)}$$
$$\times\frac{1}{(\omega/2+\mu)^2+[\nu(k_\parallel/2+q_\parallel)^2+\nu_\perp(k_\perp/2+q_\perp)^2]^2}\,.$$

The hydrodynamic limit of $\omega\to 0$ and $k_\perp\to 0$ limits can be taken right away. After integration over the internal frequency μ, we have to leading order in $k_\parallel^2$

$$\Sigma(k_\parallel)=\left[-\frac{\lambda^2 D}{4}\right]\frac{1}{(2\pi)^d}\int d^dq\,\frac{k_\parallel^2-2k_\parallel q_\parallel}{(\nu_\parallel q_\parallel^2+\nu_\perp q_\perp^2)(\nu_\parallel q_\parallel^2+\nu_\perp q_\perp^2+\nu_\parallel k_\parallel q_\parallel)}$$
$$=-\frac{\nu_\parallel k_\parallel^2}{4}\left[\frac{\lambda^2 D}{\nu_\parallel^3}\right]\left[\frac{\nu_\parallel}{\nu_\perp}\right]^{(d-1)/2}\frac{2S_{d-1}}{(2\pi)^d}\int_{k_\parallel}^{\infty}dq_\parallel q_\parallel^{d-5}\int_0^\infty dy\,y^{d-2}[(1+y^2)^{-2}+2(1+y^2)^{-3}]\,.$$

Note that the above integral is infrared divergent for $d<4$. This apparent divergence signals the relevance of nonlinearity below four dimensions; it is this type of divergences the renormalization procedure is designed to handle. For now we give the diverging integral an infrared cutoff, $k_\parallel\to 0$. In Sec. III B we show that it is only necessary to evaluate the expression for $\Sigma(k_\parallel)$ to leading order in $\epsilon=4-d$, giving the result

$$\Sigma(k,\omega)=-\frac{\nu_\parallel k_\parallel^2}{4}\left[\frac{\lambda^2 D}{\nu_\parallel^{3/2}\nu_\perp^{3/2}}\right]\frac{2S_{d-1}}{(2\pi)^d}\left[\frac{k_\parallel^{-\epsilon}}{\epsilon}\right]\frac{3\pi}{8}\,,$$

which leads to Eq. (15).

APPENDIX B: SCALING OF GLOBAL QUANTITIES

In this appendix, we take a close look at the general scaling behavior of global quantities such as the output current $J(t)$ and the energy dissipation rate $E(t)$ monitored in Sec. II B. We shall first study the case of linear diffusion, which describes the system at and above the critical dimension $d_c=4$. Afterwards, we consider extensions to the nonlinear system in Eq. (7).

If the nonlinear term in Eq. (7) is neglected, then we have a linear Langevin equation with a local current $\mathbf{j}^{(0)}(\mathbf{x},t)=\nu\nabla h$. As shown in Sec. III C, the "energy dissipation" of the system is the sum of local current, i.e., $E(t)=\int_L d^dx j(\mathbf{x},t)$. For the linear equation, the correlation function of j is easily obtained in Fourier space,

$$C_{jj}^{(0)}(\mathbf{k},\omega)=\frac{D\nu^2k^2}{\nu^2k^4+\omega^2}\,. \tag{B1}$$

To obtain the power spectrum, naively one might expect $S_E^{(0)}(\omega)=C_{jj}^{(0)}(k\to 0,\omega)$. This would generally be valid if the system were insensitive to the boundaries (say closed, with periodic boundary conditions). However, it gives a null result in this case since $\mathbf{j}^{(0)}$ is a perfect derivative. What we should do instead is to take the *open* boundary condition of the problem properly into account. A more algebraically amenable alternative is to consider the system as being a finite portion (of volume L^d) of an infinite

system. For frequencies above the finite-size cutoff $\omega_c = \nu L^{-2}$, this simplified treatment is not expected to be different from a rigorous treatment with the open boundary condition [71].

The simplified treatment amounts to writing the power spectrum as

$$S_E(\omega) = \prod_{n=1}^{d} \int_0^L dx_n \int_0^L dx_n' \int dk_n e^{ik_n(x_n - x_n')} C_{jj}(\mathbf{k},\omega)$$
$$= L^{2d} \prod_{n=1}^{d} \int dk_n \left[\frac{\sin(k_n L)}{k_n L} \right]^2 C_{jj}(\mathbf{k},\omega) .$$

The asymptotic behavior may be obtained by approximating

$$\prod_{n=1}^{d} \int dk_n \left[\frac{\sin(k_n L)}{k_n L} \right]^2 = \int \frac{d^d k}{[1+(kL)^2]^d} .$$

Using Eq. (B1), we find $S_E^{(0)}(u \equiv \omega L^2/\nu) = DL^{d+2} I_E^{(0)}(u)$, where

$$I_E^{(0)} = \int \frac{d^d y}{(1+y^2)^d} \frac{y^2}{y^4+u^2} .$$

In the region of validity and interest $u \gg 1$, the above integral is

$$I_E^{(0)} \approx \frac{1}{u^2} \int_0^{u^{1/2}} \frac{d^d y y^2}{(1+y^2)^d} + \int_{u^{1/2}}^{\infty} \frac{d^d y}{y^{2d+2}} .$$

For $d \geq 2$, the first integral is convergent, yielding $I_E^{(0)}(u) \sim u^{-2}$, while for $d < 2$, the leading contribution is $u^{-(d+2)/2}$. Hence, the $1/f$-noise exponent for "energy" is

$$\alpha_E^{(0)} = \min \left\{ 2, \frac{d+2}{2} \right\} .$$

A similar calculation can be carried out for the total output current $J(t)$, the other quantity monitored in Sec. II B. Summing up local currents at the open boundary as described in Sec. III C we have $J(t) = \int_L d^{d-1} x_\perp j(x_\parallel = L, x_\perp, t)$. The power spectrum for J is again computed using the correlation function in Eq. (B1) as

$$S_J^{(0)}(u \equiv \omega L^2/\nu) = DL^d \int dy_\parallel \int d^{d-1} y_\perp \frac{1}{(1+y_\perp^2)^{d-1}} \times \frac{y_\parallel^2 + y_\perp^2}{(y_\parallel^2 + y_\perp^2)^2 + u^2} .$$

In the limit $u \gg 1$, the leading divergence of the above integral is

$$\int_0^{u^{1/2}} dy_\parallel \int_0^{u^{1/2}} d^{d-1} y_\perp \frac{1}{(1+y_\perp^2)^{d-1}} \frac{y_\parallel^2}{u^2} \sim u^{-1/2} .$$

We find the analogous exponent for the output current to be $\alpha_J^{(0)} = \frac{1}{2}$ in all d. The exponents derived here are in agreement with those found earlier for the case $d = 3$ in Ref. [35].

With the behavior of the linear theory in mind, we now proceed to compute the power spectra for the full nonlinear problem in Eq. (7). As explained in Sec. III C the local current operator is $j(\mathbf{x},t) = h^2(\mathbf{x},t)$. In accordance with the homogeneous scaling hypothesis, the correlation function takes the form

$$C_{jj}(k_\parallel, \mathbf{k}_\perp, \omega) = k_\parallel^{-\alpha} F \left[\frac{k_\perp}{k_\parallel^\zeta}, \frac{\omega}{k_\parallel^z} \right] , \tag{B2}$$

where the exponents ζ and z are those given in Eq. (22). The other exponent, a is obtained by requiring $C_{jj} \sim \langle h^2 h^2 \rangle \sim \langle hh \rangle^2$. This gives $a = 4\chi + (d-1)\zeta + 1 + z = 2$, using exponent values in Eq. (22). In the naive scaling analysis carried out in Sec. III C, two implicit assumptions were made: (a) The power spectra are obtained from the $k \to 0$ limits of the correlation function C_{jj}; and (b) $C(k \to 0, \omega) \sim \omega^{-a/z}$ independent of k. We shall now carefully examine these two assumptions.

Since assumption (a) is not valid for the linear equation, we will again treat our system as a finite portion of an infinite one. We next assume that the scaling function $F(x,y)$ has the generalized limiting behavior $F(x \to 0, y \to 0) = \text{const}$, $F(x \to \infty, y) \to x^{-a/\zeta}$, and $F(x, y \to \infty) \to y^{-b}$. This introduces a new unknown exponent b. Assumption (b) corresponds to the special limit $b = a/z$.

Given the form of the correlation function in Eq. (B2), and the prescribed limiting behavior, the power spectra can be computed as before. The dominant contribution to the total current is

$$S_J(u) \sim \int_0^{u^{1/z}} dy_\parallel \int_0^{u^{\zeta/z}} d^{d-1} y_\perp \frac{1}{(1+y_\perp^2)^{d-1}} y^{-a} \left[\frac{u}{y_\parallel^z} \right]^{-b}$$
$$\sim u^{(1-a)/z} \text{ if } bz - a > -1, \tag{B3}$$

where $u = \omega L^z$ is the reduced frequency. Hence the $1/f$-noise exponent for total current is $\alpha_J = (a-1)/z = (7-d)/6$ (since $a = 2$). Note that this result is independent of the unknown exponent b. Also it is the same as the one obtained in Sec. III C using the most naive scaling analysis, thus explicitly demonstrating that the boundary effect is negligible in the hydrodynamic limit, and that assumption (a) is valid. Similarly, the leading contribution to the power spectrum of energy dissipation is

$$S_E(u) \sim \int_0^{u^{1/z}} dy_\parallel \frac{1}{1+y_\parallel^2} \int_0^{u^{\zeta/z}} d^{d-1} y_\perp \frac{1}{(1+y_\perp^2)^{d-1}} \times y^{-a} \left[\frac{u}{y_\parallel^z} \right]^{-b}$$
$$\sim -b \text{ if } 1 > bz - a > -1 . \tag{B4}$$

Note that if $bz - a = 0$ as in assumption (b), then $\alpha_E = b = 2/z$ is again the expression obtained from naive scaling. However, this is not necessarily the case.

We now discuss the range of values the exponent b may take. This exponent describes spatially averaged behavior of the correlation function, i.e., $C(k \to 0, \omega)$

$\rightarrow k^{bz-a}\omega^{-b}$. For systems with $C(k\rightarrow 0,\omega)\rightarrow 0$, we must have $bz-a>0$; an example is the linear problem analyzed at the beginning of this appendix. If we consider instead the height-height correlation function, the $k=0$ mode of Eq. (7) reads

$$\left.\frac{\partial h}{\partial t}\right|_{k=0}=\eta(k=0,t)\ ,$$

since the deterministic dynamics is conservative. This gives $C_{hh}(k=0,\omega)=\omega^{-2}$, and $ba-z=0$. To determine b for C_{jj}, we examine the dynamics of $j(k=0,t)=\int dx h^2(x,t)$ and find

$$\left.\frac{\partial j}{\partial t}\right|_{k=0}=\int dx\left[\left(\frac{\partial h}{\partial x}\right)^2+\eta(x,t)h(x,t)\right]$$

which is generically nonvanishing. The two integrals actually appear to diverge barring miraculous cancellation. (It is interesting to observe here that the $k=0$ mode of h^2 diverges even within the linear diffusion theory.) Hence, even though we have not been able to compute the numerical value of the exponent b, we can put an upper bound $b\leq a/z=2/z$. Also from Eqs. (B3) and (B4), we see the condition $bz-a>-1$ is needed to avoid infrared divergences. Putting these together, we have $1/z<\alpha_E\leq 2/z$.

[1] B. B. Mandelbrot, *The Fractal Geometry of Nature* (Freeman, San Francisco, 1982).

[2] See, e.g., W. H. Press, Comments Mod. Phys. C **7**, 103 (1978); P. Dutta and P. M. Horn, Rev. Mod. Phys. **53**, 497 (1981); J. J. Brophy, J. Appl. Phys. **40**, 3551 (1969).

[3] K. L. Schick and A. A. Vereen, Nature (London) **251**, 599 (1974).

[4] B. B. Mandelbrot and J. W. Van Ness, SIAM Rev. **10**, 422 (1968).

[5] S.-K. Ma, *Modern Theory of Critical Phenomena* (Benjamin-Cummings, Reading, MA, 1976).

[6] P. Bak, C. Tang, and K. Wiesenfeld, Phys. Rev. Lett. **59**, 381 (1987); Phys. Rev. A **38**, 364 (1988).

[7] See, for example, *Phase Transitions and Critical Phenomena,* edited by C. Domb and M. S. Green (Academic, London, 1976), Vol. 6.

[8] M. Kardar, G. Parisi, and Y.-C. Zhang, Phys. Rev. Lett. **56**, 889 (1986).

[9] A detailed discussion of possible relations between SOC and Goldstone modes can be found in S. P. Obukhov, Phys. Rev. Lett. **65**, 1395 (1990).

[10] By $1/f$ noise, we mean noise with any power spectra $S(f)\sim 1/f^{\alpha}$ where $0<\alpha<2$. Such noise is more erratic than Brownian noise ($1/f^2$) but more orderly than uncorrelated white noise (f^0).

[11] J. M. Carlson and J. S. Langer, Phys. Rev. Lett. **62**, 2632 (1989); Phys. Rev. A **40**, 6470 (1989).

[12] H. M. Jaeger, C.-H. Liu, and S. R. Nagel, Phys. Rev. Lett. **62**, 40 (1989).

[13] P. C. Hohenberg and B. I. Halperin, Rev. Mod. Phys. **49**, 435 (1977), and references therein.

[14] L. P. Kadanoff, S. R. Nagel, L. Wu, and S. M. Zhou, Phys. Rev. A **39**, 6524 (1989).

[15] C. Tang and P. Bak, Phys. Rev. Lett. **60**, 2347 (1988).

[16] B. Grossmann, H. Guo, and M. Grant, Phys. Rev. A **40**, 6763 (1989).

[17] S. S. Manna, J. Stat. Phys. **59**, 509 (1990).

[18] P. Grassberger and S. S. Manna, J. Phys. (Paris) **51**, 1077 (1990).

[19] J. M. Carlson, J. T. Chayes, E. R. Grannan, and G. H. Swindle, Phys. Rev. A **42**, 2467 (1990).

[20] H. J. Jensen, K. Christensen, and H. C. Fogedby, Phys. Rev. B **40**, 7425 (1989); K. Christensen, H. C. Fogedby, and H. J. Jensen, J. Stat. Phys. **63**, 653 (1991).

[21] J. Kertész and L. B. Kiss, J. Phys. A **23**, L433 (1990).

[22] B. B. Mandelbrot and J. R. Wallis, Water Resour. Res. **5**, 321 (1969).

[23] The exponent σ' associated with the finite-size scaling of the power spectra should not be interpreted as the dynamic exponent σ because the cutoff time (T_A of Fig. 6) is due to the overlap of avalanches, which in turn depends on the input rate $J_{\rm in}$. We expect T_A to have different L dependences for input rates with different L scalings. The dynamic exponent σ is usually obtained from the finite-size scaling of the power spectra in the nonoverlapping limit. This, however, has not been pursued here since our interest lies in the overlapping avalanche limit.

[24] S. P. Obukhov, in *Random Fluctuations and Pattern Growth: Experiments and Models,* edited by H. E. Stanley and N. Ostrowsky (Kluwer, Dordrecht, 1988).

[25] D. Dhar and R. Ramaswamy, Phys. Rev. Lett. **63**, 1659 (1989).

[26] D. Dhar, Phys. Rev. Lett. **64**, 1613 (1990).

[27] Note that z is the dynamic exponent for the *interacting* avalanches, different from σ which is the dynamic exponent for a *single* avalanche.

[28] Since $T_B\sim L^z$, there may be an *uncorrelated* interval between T_B and T_C for $z<2$. See Fig. 6.

[29] T. Hwa and M. Kardar, Phys. Rev. Lett. **62**, 1813 (1989).

[30] G. Grinstein and D.-H. Lee, Phys. Rev. Lett. **66**, 177 (1991).

[31] H. K. Janssen and B. Schmittmann, Z. Phys. B **63**, 517 (1986).

[32] This is in essence the summability of Eq. (10), and is otherwise known as the renormalizability hypothesis. An example of such sums can be found in B. Duplantier, T. Hwa, and M. Kardar, Phys. Rev. Lett. **64**, 2022 (1990).

[33] D. Forster, D. R. Nelson, and M. J. Stephen, Phys. Rev. A **16**, 732 (1977).

[34] E. Medina, T. Hwa, M. Kardar, and Y.-C. Zhang, Phys. Rev. A **39**, 3053 (1989).

[35] R. F. Voss and J. Clarke, Phys. Rev. B **13**, 556 (1976). See also S. H. Liu, Phys. Rev. B **16**, 4218 (1977).

[36] J. M. Carlson, J. T. Chayes, E. R. Grannan, and G. H. Swindle, Phys. Rev. Lett. **65**, 2547 (1990).

[37] A condensed version of these arguments appears in M. Kardar, in *Disorder and Fracture,* edited by J. C. Charmet, S. Roux, and E. Guyon (Plenum, New York, 1990), p. 3.

[38] G. Grinstein, S. Sachdev, and D. H. Lee, Phys. Rev. Lett. **64**, 1927 (1990).

[39] P. L. Garrido, J. L. Lebowitz, C. Maes, and H. Spohn, Phys. Rev. A **42**, 1954 (1990); Z. Cheng, P. L. Garrido, J.

L. Lebowitz, and J. L. Valles, Europhys. Lett. **14**, 507 (1991).
[40] J. Villain, J. Phys. I **1**, 19 (1991).
[41] Z.-W. Lai and S. Das Sarma, Phys. Rev. Lett. **66**, 2348 (1991).
[42] D. Wolf and J. Villain, Europhys. Lett. **13**, 389 (1990).
[43] S. S. Manna, L. B. Kiss, and J. Kertész, J. Stat. Phys. **64**, 923 (1990).
[44] W. J. Yeh and Y. H. Kao, Phys. Rev. Lett. **53**, 1590 (1984).
[45] H. J. Jensen, Phys. Rev. Lett. **64**, 3103 (1990).
[46] G. Grinstein, T. Hwa, and H. J. Jensen, Phys. Rev. A **45**, R559 (1992).
[47] G. I. Sivashinsky and D. M. Michelson, Prog. Theor. Phys. **63**, 2112 (1980).
[48] Y. Kuramoto and T. Tsuzuki, Prog. Theor. Phys. **55**, 356 (1976); G. I. Sivashinsky, Acta Astronautica **6**, 569 (1979), and references therein.
[49] S. Zalesky, Physica D **34**, 427 (1989).
[50] J. Toner, Phys. Rev. Lett. **66**, 679 (1991).
[51] K. L. Babcock and R. M. Westervelt, Phys. Rev. Lett. **64**, 2168 (1990).
[52] X. Che and H. Suhl, Phys. Rev. Lett. **64**, 1670 (1990).
[53] P. Evesque and J. Rajchenbach, C. R. Acad. Sci. Ser. 2 **307**, 223 (1988).
[54] G. A. Held, D. H. Solina, D. T. Keane, W. J. Haag, P. M. Horn, and G. Grinstein, Phys. Rev. Lett. **65**, 1120 (1990).
[55] H. M. Jaeger, C.-H. Liu, S. R. Nagel, and T. A. Witten, Europhys. Lett. **11**, 619 (1990).
[56] J. Rajchenbach, Phys. Rev. Lett. **65**, 2221 (1990).
[57] See A. Mehta, in *Correlation and Connectivity in Physics and Biology,* edited by H. E. Stanley and N. Ostrowsky (Kluwer, Dordrecht, 1990), and references therein.
[58] A. Sornette and D. Sornette, Europhys. Lett. **9**, 197 (1989).
[59] P. Bak and C. Tang, J. Geophys. Res. **94**, 15 635 (1989).
[60] P. Bak and K. Chen, in *Nonlinear Structure in Physical Systems—Pattern Formation, Chaos and Waves,* edited by L. Lam and H. C. Morris (Springer, New York, 1990).
[61] K. Chen, P. Bak, and S. P. Obukhov, Phys. Rev. A **43**, 625 (1991).
[62] J. M. Carlson, J. Geophys. Res. **96**, 4255 (1991); J. M. Carlson, J. S. Langer, B. E. Shaw, and C. Tang, Phys. Rev. A **44**, 896 (1991); B. Shaw, J. M. Carlson, and J. S. Langer (unpublished).
[63] C. H. Scholtz, in *Spontaneous Formation of Space-Time Structures and Criticality,* edited by T. Riste and D. Sherrington (in press).
[64] S. N. Majumdar and D. Dhar (unpublished).
[65] L. P. Kadanoff, A. B. Chabra, A. J. Kolan, M. J. Feigenbaum, and I. Procaccia (unpublished).
[66] H. J. S. Feder and J. Feder, Phys. Rev. Lett. **66**, 2669 (1991); **67**, 283 (1991).
[67] L. M. Sander and H. Yan, Phys. Rev. A **44**, 4885 (1991).
[68] J. Krug, Phys. Rev. A **44**, 801 (1991).
[69] P. Bak, K. Chen, and M. Creutz, Nature (London) **342**, 780 (1990).
[70] C. H. Bennett and M. S. Bourzutschky (unpublished).
[71] This is also the treatment used in Ref. [35]. The result agrees with the numerical simulation of linear diffusive processes. It has also been verified experimentally in J. H. Scofield and W. W. Watt, Phys. Rev. Lett. **54**, 353 (1985).

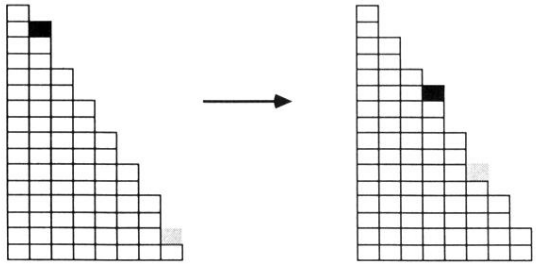

FIG. 16. The joint inversion symmetry $h \rightarrow -h$ and $x_{\parallel} \rightarrow -x_{\parallel}$: $+h$ (filled block) moves down the slope while $-h$ (void, shaded block) moves uphill.

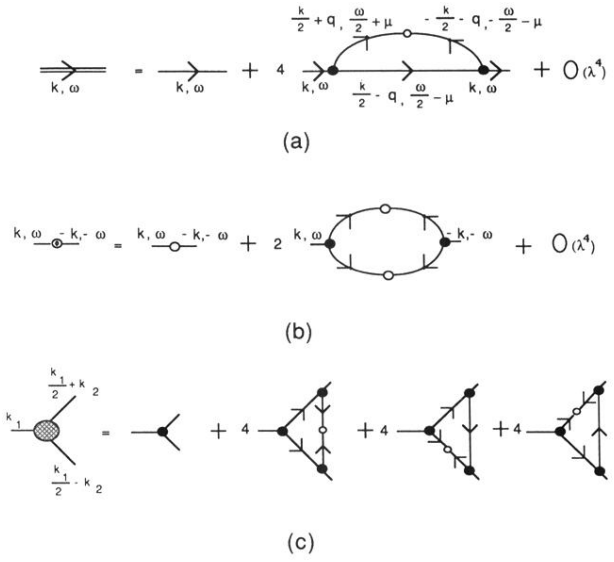

FIG. 18. After averaging over the noise, the perturbation series of Eq. (13) can be reorganized to describe (a) a renormalized propagator, (b) a renormalized noise spectrum, and (c) a renormalized vertex function (or interaction parameter).

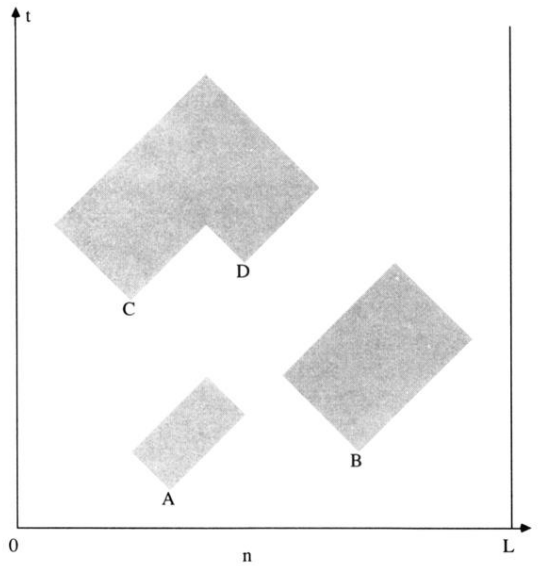

FIG. 2. One-dimensional avalanche processes represented in a space-time diagram. The two avalanches initiated at points A and B are considered independent because they do not overlap in space time. The two initiated at points C and D, however, do overlap.

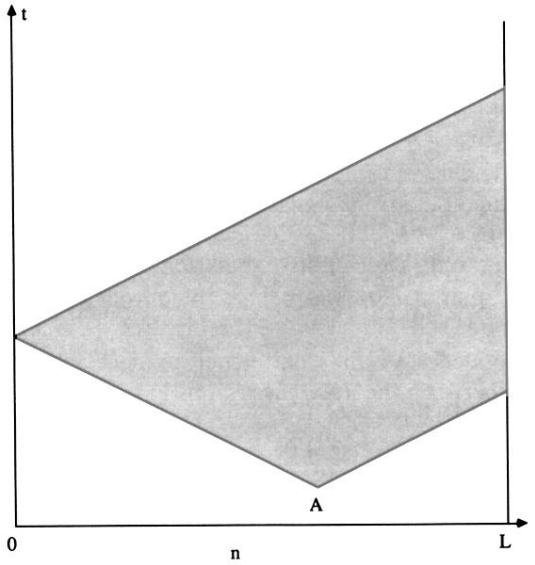

FIG. 9. A space-time diagram for a discharge event initiated at point A.